OPTIMISATION OF LITHIUM-ION BATTERY CHARGING PROFILES USING A THERMAL AND HEALTH-AWARE FUZZY LOGIC STRATEGY

BY:

UDE-NATHA IFEANYICHUKWU SALVATION

ENG2006276

ELECTRICAL/ELECTRONIC ENGINEERING

FACULTY OF ENGINEERING

UNIVERSITY OF BENIN

A PROJECT SUBMITTED TO THE DEPARTMENT OF ELECTRICAL/ELECTRONIC ENGINEERING, FACULTY OF ENGINEERING, UNIVERSITY OF BENIN,
IN PARTIAL FULFILLMENT OF THE REQUIREMENTS FOR THE AWARD OF THE BACHELOR OF ENGINEERING(B.ENG.) DEGREE IN ELECTRICAL/ELECTRONIC ENGINEERING.

OCTOBER, 2025

CERTIFICATION

We, the undersigned, certify that this work was carried out by UDE-NATHA IFEANYICHUKWU SALVATION in the Department of Electrical/Electronic Engineering, Faculty of Engineering, University of Benin, Benin City. For the requirements of the award of Bachelor of Engineering (B.ENG.) Degree in Electrical/Electronic Engineering

---------- ----------

Engr. A.P Oriaifo Date

(Project Supervisor)

---------- ----------

Engr. Dr. S.O Omorogiuwa Date

(Head of Department)

DEDICATION

With profound gratitude, I dedicate this project work to God Almighty for being my strength and help. Indeed, by God, I have run over a troop, and I have leaped over a wall. I also dedicate this project to my parents, Mr. A. O. Ude-Natha and Mrs. Helen Uchenye Ude-Natha. I am forever grateful for your support through this period.

ACKNOWLEDGEMENT

To God Almighty, your divine grace and unwavering presence in my life have been a constant source of strength and inspiration. I am profoundly thankful for the blessings, wisdom, and inner strength You have provided, guiding me through this great journey.

To the Head of Department (HOD), Engr. Dr. S. O. Omorogiuwa, your exemplary leadership, unwavering encouragement, and steadfast commitment to academic excellence have profoundly shaped my academic and research journey. Thank you for all you do for every student in the department, and for being a father figure.

I extend my sincere appreciation to my supervisor, Engr. A. P. Oriaifo, for his invaluable mentorship, patience, and expertise. Your guidance has been instrumental in refining my research skills and shaping the direction of this project. Your dedication to my success has been a driving force behind these achievements.

A big shout-out to my parents, Mr. Ambrose & Mrs. Helen Ude-Natha; my siblings, Precious, Favour, Anita, and God'spower; and my extended family for their significant financial contributions, unwavering love, encouragement, and prayers throughout this journey. God bless you all; I love you all.

A big thank you to everyone who prayed for me and supported me financially throughout this phase. God bless and increase you all.

I will also not fail to appreciate my course-mates, senior colleagues, and my dear friend, Abraham Okoye, for their immense support and encouragement. This appreciation will not be complete without acknowledging Richard for his immense support during this final phase. God bless you.

TABLE OF CONTENTS

LIST OF TABLES

LIST OF FIGURES

ABSTRACT

This study addresses the critical challenge of optimizing charging performance in lithium-ion batteries (LIB) by designing and analysing an intelligent Battery Management System (BMS) with an adaptive Fuzzy Logic Controller (FLC). The research aims to resolve the trade-off between charging speed, thermal safety, and cycle life longevity by moving beyond rigid Constant Current–Constant Voltage (CC-CV) methods to a holistic, health-aware control strategy. The FLC was engineered to integrate three key active parameters: State of Charge (SOC), State of Health (SOH), and Temperature, as inputs to dynamically regulate the charging current (I_c) and voltage (V_c).

The methodology adopted a quantitative simulation-based experimental design using the MATLAB/Simulink environment. A high fidelity Second-Order Equivalent Circuit Model (ECM) of the Molicel INR–21700–P45B cell was formulated to replicate realistic electro-thermal dynamics. A central component of the study involved a systematic comparative analysis of two different Membership Function (MF) types within the FLC: Triangular and Gaussian. This approach allowed for rigorous stress testing under diverse conditions, including varied SOC levels, degradation states (100% vs. 95% SOH), and a wide ambient temperature range (0°C to 55°C).

The results demonstrated the definitive superiority of the Gaussian-type MF, which produced significantly smoother control transitions, minimized current ripple, and reduced electrical stress compared to the Triangular MF. The Gaussian-based FLC successfully maintained charging efficiency within the optimal thermal window (25°C to 45°C) and demonstrated a critical "Survival Mode" at 55°C, where it autonomously throttled the charging current by approximately 63% to prevent thermal runaway. Furthermore, the integration of SOH allowed the controller to intelligently derate current for aged cells, confirming its capability as a robust, safety-first solution for next-generation intelligent BMS architectures.

CHAPTER ONE – INTRODUCTION

1.1. BACKGROUND OF THE STUDY

The rapid global transition toward electrified transportation, renewable energy integration, and sustainable storage solutions has made the performance, safety, and longevity of rechargeable batteries a priority for researchers and industry stakeholders alike (Hannan, M.A. et al., 2017; Liu, K. et al., 2019). Among the various battery chemistries available today, lithium-ion (Li-ion) batteries dominate applications such as electric vehicles (EVs), grid-scale renewable storage systems, portable electronics, and unmanned aerial systems due to their high energy density, long cycle life, and favourable power-to-weight ratio. (Zubi, G. et al., 2018; Gong, A. et al., 2023; Diouf, B. & Pode, R., 2015).

However, optimising the performance of these batteries requires precise management. The battery management system (BMS) acts as the "brain" of the storage unit, supervising key parameters such as state of charge (SOC), state of health (SOH), temperature, and current flow. While basic BMS functions ensure the battery stays within safe voltage limits, advanced BMS architecture must manage the complex trade-offs between charging speed, thermal safety, and cycle life longevity (Hannan, M.A. et al., 2017; Liu, K. et al., 2019).

A critical challenge in modern BMS design is regulating the charging profile. Traditional methods, such as Constant Current–Constant Voltage (CC-CV), are rigid and often fail to account for dynamic internal conditions, such as temperature fluctuations and degradation (aging). For instance, applying a standard high current to an aged or overheated cell can accelerate degradation mechanisms, such as lithium plating or Solid Electrolyte Interphase (SEI) growth. Consequently, there is a growing need for intelligent charging control strategies that can adaptively regulate current based on the real-time health and environmental state of the battery (Zhang, C. et al., 2021; Li, J. et al., 2020; Farmann, A. et al., 2015).

Fuzzy Logic Control (FLC) has emerged as a powerful tool for this purpose. Rooted in Lotfi Zadeh's theory of fuzzy sets, FLC enables control decisions based on linguistic rules (e.g., "if Temperature is High, then Current is Low") rather than precise, computationally heavy mathematical models. Recent studies have demonstrated the effectiveness of fuzzy logic in managing battery nonlinearities. For example, Murdianto et al. (2024) and Shaout and Brauchler (2025) explored intelligent control to improve

system response times (Zadeh, L.A. et al. (1965), Murdianto, F.D. et al. (2024), Shaout, A. & Brauchler, M. (2025)).

Despite these advances, most research focuses heavily on converter topologies while overlooking the optimisation of the control logic itself—specifically, how the choice of membership functions (e.g., Triangular vs. Gaussian) and integration of health parameters (SOH) impact the safety and efficiency of the charging process (Kumar, R. & Singh, S. (2020)). Simulation remains the most practical platform for advancing this research, allowing for the rigorous testing of thermal extremes and degradation scenarios that are difficult to replicate consistently in physical hardware (Tran, M.K., & Fowler, M. (2020)).

1.2. RESEARCH PROBLEM

Intelligent charging control based on fuzzy logic represents a promising approach to enhancing the safety and lifetime of lithium-ion batteries. However, several research challenges remain sufficiently addressed in the existing literature:

1.2.1. Neglect of Environmental Stressors in Simulation: The majority of simulation-based studies neglect temperature effects that strongly influence cell behaviour. Standard models often assume a constant ambient temperature, failing to capture critical scenarios where a BMS must actively throttle current to prevent thermal runaway. This study addresses this by explicitly modelling performance across a wide thermal window (0^oC to 55^oC)

1.2.2 Lack of Health – Aware Control Logic: Many existing controllers rely solely on Voltage and SOC thresholds, disregarding the State of Health (SOH). As batteries age, their internal resistance increases and capacity fades. A controller that does not account for SOH will aggressively charge an aged battery, leading to accelerated failure. The integration of SOH into the control loop remains a critical but often unresolved requirement.

1.2.3. Insufficient Analysis of Membership Function (MF) impact: While fuzzy logic is widely used, there is limited analysis comparing how different Membership Functions shape affects control smoothness and stability. Most studies default to Triangular MFs for simplicity. However, abrupt transitions in control logic can cause current ripples that stress battery chemistry. This study identifies a gap in quantitatively comparing Gaussian vs. Triangular MFs for battery applications.

1.2.4. Trade-off Between Charging Speed and Safety: A significant challenge persists in balancing the desire for "fast charging" (high C-rates) with the need for thermal safety. Static algorithms cannot navigate this trade-off dynamically. There is a need for an adaptive system that can maximise charging speed in safe conditions (e.g., 35^{o}C) while automatically entering a "survival mode" in critical conditions (e.g., 55^{o}C or 0^{o}C)

1.3 RESEARCH QUESTION

These limitations motivate the central research question of this study:

"How can a multi-objective fuzzy logic controller be designed and modelled to optimise the charging profile of lithium-ion batteries, specifically to enhance thermal safety, energy efficiency, and degradation adaptation (SOH), compared to conventional control methods?"

To answer this, the study poses the following specific sub-questions:

1. Does the integration of SOH and Temperature inputs into a fuzzy controller effectively mitigate thermal stress during charging?
2. How does the selection of Membership Function shape (Gaussian vs. Triangular) impact the smoothness, stability, and response time of the charging current?
3. Can an adaptive controller successfully optimise the trade-off between charging speed (C-rate) and safety limits under extreme environmental conditions (e.g., 55^{o}C)?

1.4. AIMS AND OBJECTIVES OF THE STUDY

1.4.1. Aim of the Study

The primary aim of this research is to design, model, and simulate an intelligent Fuzzy Logic-based charging controller for a Lithium-Ion battery (specifically the Molicel INR-21700-P45B). The study seeks to develop a control strategy that dynamically adapts charging current and voltage based on real-time thermal and health conditions, thereby solving the trade-off between charging speed, safety, and cycle life longevity.

1.4.2. Specific Objectives

To achieve this aim, the following specific objectives were established:

1. To develop a high-fidelity electro-thermal model of the lithium-ion battery in the MATLAB/Simulink environment.

2. To design a multi-input Fuzzy Inference System (FIS) that utilizes SOC, SOH, and Temperature to regulate the charging process.
3. To implement the complete intelligent charging architecture in Simulink, establish a closed-loop feedback system.
4. To validate the system's performance by benchmarking the proposed controller against standard charging protocols and subjecting it to thermal stress tests.

1.5. METHODOLOGY

To achieve the objectives of this study, a structured, simulation-based methodology was adopted using the MATLAB/Simulink environment. The research was carried out in four distinct phases:

1. A high-fidelity Second-Order Equivalent Circuit Model (ECM) was formulated to replicate the electrochemical dynamics of the Molicel INR-21700-P45B lithium-ion cell, capturing transient polarisation effects and internal resistance characteristics. (Chapter 3, Section 3.2)
2. The intelligent control logic was established using a Fuzzy Inference System (FIS) that utilises State of Charge (SOC), State of Health (SOH), and Temperature, mapped to a comprehensive rule base of 125 rules to determine optimal charging current (Chapter 3, Section 3.5).
3. The complete closed-loop charging architecture was developed in Simulink, integrating the controller with the battery plant model and a Thermal-Electrical coupling feature to simulate realistic Joule heating and temperature rise (Chapter 3, Section 3.6).
4. The system was subjected to rigorous stress testing under varying ambient temperatures (0°C, 25°C, 35°C, 45°C & 55°C) and degradation states (100% vs. 95% SOH) to quantitatively compare the stability and safety performance of Gaussian Membership Functions against the standard Triangular benchmark (Chapter 4, Section 4.2).

1.6. SIGNIFICANCE OF THE RESEARCH

Addressing the above research question carries substantial significance for both the scientific community and industry practitioners.

From a technical standpoint, this research advances the state-of-the-art in intelligent BMS design by demonstrating the superiority of Gaussian Membership Functions over

traditional Triangular forms. The results provide evidence that Gaussian MFs offer smoother control surfaces, reducing the “chattering” or current ripples that can harm battery electrodes (Olunloyo, V.O.S. et al. (2014), Breugelmans, T. et al. (2016), Felix, C. et al. (2023)). Furthermore, the development of the health-aware (SOH) controller ensures that charging protocols evolve as the battery ages, a critical feature for extending the usable life of second-life EV batteries.

From an industry perspective, the study validates a “Safety-First” control logic. By simulating extreme temperatures (0^{o}C and 55^{o}C), the research demonstrates a control framework capable of preventing thermal runaway through autonomous current throttling. This directly contributes to safer electric vehicle operation and more reliable renewable energy storage systems in harsh climates (Liu, K. et al. (2023), Olabi, A.G. et al. (2022)).

From an environmental perspective, prolonging battery life through optimised charging reduces the frequency of pack replacements, thereby lowering the demand for raw materials such as lithium, cobalt, and nickel. This mitigates the environmental impact of mining and reduces the volume of spent batteries requiring recycling (Tarpeh, W. & Bunke, S. (2025), Campbell, M. & Sverdrup, H. (2023)).

Ultimately, this project shifts the focus from simple “voltage balancing” to holistic charging optimisation, proving that intelligent software can significantly enhance the performance of battery hardware without requiring expensive circuit modifications (Hannan, M.A. et al (2017), Shaout, A. & Brauchler, M. (2025)).

CHAPTER TWO – LITERATURE REVIEW

2.1. OVERVIEW OF RELEVANT LITERATURE

The theoretical basis for fuzzy logic applications in control systems emerged well before its adoption in battery management. Klawonn and Klement (1999) conducted a mathematical analysis of fuzzy classifiers, illustrating how fuzzy rules can provide solutions to classification problems where crisp, binary logic fails, particularly in cases with imprecise or overlapping data boundaries. Although the context was pattern classification, the implications for control systems were significant: fuzzy logic could manage uncertainty, handle nonlinear relationships, and provide adaptive decision making without requiring precise mathematical models of the system. These properties make fuzzy logic a natural fit for battery management, where parameters like state of charge (SOC), state of health (SOH), and temperature are difficult to model with absolute precision.

The first decade of the 2000s also saw a shift in battery research from purely dissipative (passive) balancing methods to approaches that aimed to conserve energy and increase efficiency. A landmark contribution came from Einhorn, Conte, and Fleig (2010)**,** who challenged the prevailing voltage-based balancing approach by advocating for energy-based balancing**.** Using Modelica/Dymola simulations validated with empirical measurements on a three-cell lithium-ion battery pack, they demonstrated that energy-based balancing increased usable energy by 32%, compared to 27% for voltage-based methods. However, the study acknowledged that energy-based strategies required accurate capacity and SOC estimation, a persistent difficulty due to cell ageing and temperature fluctuations.

While this study focuses on control logic, understanding the hardware constraints is essential. The early 2010s were marked by the development of sophisticated active topologies. Daowd et al. (2013) investigated switched capacitor (SC) systems, finding that while they offered high efficiency in terms of energy loss, they suffered from long equalisation times as the voltage difference between cells decreased.

Lozano et al. (2013) explored using MOSFETs in their saturation region as programmable resistors, achieving fast management with minimal energy loss (~10%). Later, Teja and Prabhaharan (2015) combined inductor-based buck–boost topologies with microcontrollers to create smart BMS architectures. Despite these hardware

successes, researchers noted that hardware complexity often outpaced control intelligence, creating a need for smarter algorithms to manage these circuits.

As hardware matured, the focus shifted to "Intelligent Control." Naguib, Kollmeyer, and Emadi (2017) concluded that converter-based active systems were most effective for EV applications but recommended the integration of SOC estimation into control, enabling decisions based on accurate cell states rather than solely on voltage readings. Omariba, Zhang, and Sun (2017) extended this by reviewing real-world operating conditions, noting that environmental stressors like temperature were rarely incorporated into simulation models or control strategies. This gap led to the development of more complex algorithms. Ouyang et al. (2018) proposed a consensus-based SOC algorithm using graph theory, which reduced time by 73%. However, the reliance on integer programming introduced computational demands challenging for real-time embedded implementation.

The most recent literature focuses on refining fuzzy logic for better precision. Zenk and Ertugral (2023) developed a fuzzy-based BMS adaptable to multiple battery chemistries. Zanella et al. (2023) applied fuzzy Q-learning for EV energy management, improving efficiency but remaining limited to simulation.

Crucially, recent contributions have begun to optimize the internal mechanics of fuzzy controllers. Murdianto et al. (2024) used an Adaptive Neuro-Fuzzy Inference System (ANFIS) to control bidirectional converters, demonstrating reduced times but lacking a detailed energy efficiency analysis. Shaout and Brauchler (2025) developed a modified fuzzy logic controller integrated with a SEPIC converter, achieving faster regulation and better voltage uniformity compared to traditional FLCs. Despite these improvements, the absence of detailed energy loss analysis and environmental testing left important performance questions unanswered.

2.2. KEY THEORIES OR CONCEPTS

2.2.1. Fundamentals of Fuzzy Logic Control

Fuzzy logic is a form of many-valued logic introduced by Lotfi Zadeh in 1965, designed to handle the concept of partial truth, that is, where truth values can range between completely true and completely false. In control systems, fuzzy logic is particularly useful in dealing with uncertainties, nonlinearities, and imprecise information. Unlike binary logic, which operates with discrete “0” or “1” values, fuzzy logic represents

variables with degrees of membership in fuzzy sets, allowing a more flexible and human-like approach to decision-making.

A typical FLC comprises four key components:

2.2.1.1. Fuzzification: Converts crisp input values (e.g., Voltage, SOC, Temperature) into degrees of membership within predefined fuzzy sets. For instance, a voltage deviation of 0.08 V may simultaneously belong to the “Low” deviation set with a membership degree of 70% and to the “Medium” deviation set with a membership degree of 30%.

2.2.1.2. Rule Base: Contains a collection of linguistic if–then rules formulated from expert knowledge or empirical observations, which define the control behaviour of the system.

2.2.1.3. Inference Engine: Evaluates the fuzzified inputs using inference mechanisms such as Mamdani or Takagi–Sugeno methods to generate fuzzy output sets.

2.2.1.4. Defuzzification: Converts these fuzzy outputs into crisp control signals, such as an exact pulse-width modulation (PWM) duty cycle for current regulation.

2.2.2. Membership Function (MF) Design

The shape of the Membership Function (MF) is a critical design parameter. Hameed et al. (2025) investigated the effect of MF shapes on BMS performance, concluding that Gaussian MFs outperformed triangular ones in terms of charging efficiency and temperature control. This finding implies that Gaussian MFs produce smoother control outputs and better temperature regulation. Similarly, Ibrahim et al. (2025) demonstrated that optimising the rule base could yield 23.5% long-term cost savings, a principle directly applicable to BMS strategies.

2.2.3. State of Health (SOH) Integration

Understanding cell imbalance and aging is essential for effective control. Imbalance arises from manufacturing variations, temperature gradients, and cycling-induced aging. These factors interact in complex ways; for instance, capacity fade (SOH decrease) changes the effective charging rate a battery can safely handle. Naguib et al. (2017) and Balasingam et al. (2020) advocated for integrated systems where control strategies are linked to SOH estimation, ensuring that energy transfer decisions are based on the battery's actual health rather than just voltage.

2.2.4. Thermal Dynamics and Environmental Stress

Temperature gradients can cause localized overcharging or undercharging, accelerating degradation. Omariba et al. (2017) found that while active management improved life in principle, environmental stressors were rarely incorporated into simulation models. Effective strategies must be adaptive, responding to changes in cell characteristics as operating conditions vary.

2.2.5. Active Energy Management Architectures

While early BMS designs relied on passive balancing, which dissipates excess energy as heat through resistors, modern high-efficiency applications utilize active energy management architectures. These systems employ power electronic circuits to actively transfer energy, theoretically improving pack efficiency and capacity utilization.

However, the hardware topology alone is insufficient. As noted by Daowd et al. (2013), switched-capacitor methods offer simplicity but suffer from slow equalization times when voltage differences are small. Conversely, inductor-based or converter-based topologies (such as Buck-Boost or SEPIC converters) allow for precise current regulation but introduce significant control complexity. The consensus in the literature is that while active architectures provide the physical capability to regulate current dynamically, their effectiveness is entirely dependent on the intelligence of the control strategy driving them. This necessitates the move from simple threshold-based logic to advanced algorithmic control.

2.2.6. Intelligent Control Strategies

To manage the non-linear dynamics of Lithium-Ion batteries, researchers have increasingly moved beyond classical control methods toward intelligent strategies.

Proportional-Integral-Derivative (PID) controllers are common but rigid. They struggle to adapt to the highly non-linear behaviour of batteries, particularly under varying thermal conditions, where a fixed gain may lead to overshoot or instability.

Adaptive Neuro-Fuzzy Inference Systems (ANFIS) and Neural Networks offer high precision and predictive capabilities. However, Murdianto et al. (2024) and Ouyang et al. (2018) note that these methods often require significant computational resources and extensive training data, making them challenging to implement on low-cost, real-time embedded BMS microcontrollers.

FLC has emerged as a robust solution because it mimics human reasoning using linguistic rules (e.g., "If Temperature is High, then Current is Low"). This allows it to handle imprecise data and adapt to varying environmental conditions without requiring complex mathematical models of the system. This study focuses on FLC because it offers the optimal balance between computational feasibility and control sophistication.

2.2.7. SOC and SOH Integration for Health-Aware Control

Accurate estimation of state-of-charge (SOC) and state-of-health (SOH) is fundamental to safe battery management.

SOC Integration: Traditional charging methods often rely on voltage thresholds. However, voltage is a poor indicator of stored energy during high-current charging due to polarization effects. Naguib et al. (2017) emphasized that integrating SOC estimation directly into the control loop allows the BMS to transition between charging phases more accurately, preventing overcharging.

SOH (Aging) Integration: As batteries age, their internal resistance increases and capacity fades. A critical gap in current literature is that many controllers "fly blind" regarding health; they apply the same aggressive current to an aged battery as they would to a new one. Balasingam et al. (2020) advocated for integrated systems where control strategies are linked to SOH, ensuring that energy transfer decisions are based on the battery's actual health. Integrating SOH as a control input, as proposed in this study, allows the BMS to derate current for aged cells, mitigating degradation risks.

2.3. GAPS OR CONTROVERSIES IN THE LITERATURE

2.3.1. Neglect of Environmental and Aging Effects

The majority of reviewed studies, particularly those relying on simulation, do not consider temperature variation, humidity, or long-term aging in their control designs. For example, Omariba et al. (2017) highlighted that few studies incorporate these factors into control algorithms. Ignoring these effects risks producing algorithms that perform well in laboratory conditions but degrade in effectiveness under real-world stresses.

2.3.2. Limited Energy Efficiency and Loss Analysis

A recurring omission in the literature is the absence of detailed energy loss breakdowns. Studies such as Shaout and Brauchler (2025) report faster performance but do not

quantify overall energy efficiency or conversion losses. In high-energy systems, even a small percentage loss can translate to significant wasted energy over time.

2.3.3. Incomplete Integration of SOC/SOH Estimation

Although the importance of integrating SOC and SOH estimation is well-documented (Einhorn et al., 2010; Naguib et al., 2017), many studies still use voltage-based thresholds as the primary balancing trigger. Problems with voltage-based control include the fact that voltage is an unreliable indicator of SOC during charging and discharging due to polarisation effects. Furthermore, Shaout and Brauchler (2025) improved control smoothness but did not integrate SOH estimation, meaning that aging effects remained unaddressed.

2.3.4. Computational Complexity vs Performance

Advanced strategies like graph-theoretic consensus (Ouyang et al., 2018) or ANFIS (Murdianto et al., 2024) offer theoretical benefits but come with high computational costs. This creates a controversy between academic feasibility and industrial feasibility, where embedded BMS controllers have limited processing power. There is a clear need for methods that optimize algorithms without significantly reducing performance.

In summary, the literature reveals significant progress in active management techniques but highlights a critical need for holistic control strategies. Current research often optimizes for speed or topology while neglecting the crucial interplay between Membership Function design, Thermal Safety, and State of Health (SOH). This study addresses these specific gaps by designing an adaptive fuzzy logic controller that explicitly integrates these parameters to ensure robust, health-aware, and environmentally stable charging.

CHAPTER THREE – METHODOLOGY

3.1. METHODOLOGY

This chapter details the methodological framework adopted for the study. The central aim is to provide a structured approach for investigating how Intelligent Fuzzy Logic Control can optimise the charging profile of lithium-ion batteries under varying thermal and health conditions. In order to achieve this, the chapter details the research design, data collection methods, system modelling, and data analysis techniques applied throughout the investigation.

The methodological choices were guided by the need to ensure both the validity and reliability of the findings, while also aligning with the research objectives outlined in Chapter One. Given the non-linear nature of battery dynamics and the risks associated with testing extreme thermal conditions on physical hardware, this study adopts a quantitative simulation-based research design using MATLAB/Simulink 2023b as the primary development and testing environment. This choice enables controlled experimentation under complex conditions, specifically extreme temperatures (-20°C to 55°C) and degradation states (SOH) that are difficult to replicate consistently in physical hardware.

Finally, the section on data analysis outlines how the results were interpreted to evaluate the performance of the fuzzy logic controller. Key performance indicators such as charging time, control smoothness, energy efficiency, and thermal stability are employed to assess the effectiveness of the proposed control strategy. Together, these methodological steps form a rigorous framework that supports the credibility of the study's conclusions and ensures that the findings are relevant for both academic and practical applications.

3. 2. RESEARCH DESIGN

The research employs an experimental simulation design. This design is appropriate because the work focuses on testing and validating an improved intelligent charging algorithm for a Battery Management System (BMS). The design involves modelling battery cells using Equivalent Circuit Models (ECM), applying fuzzy logic–based control, and comparing performance metrics (such as voltage smoothness, thermal stability, and charging time) against conventional control methods.

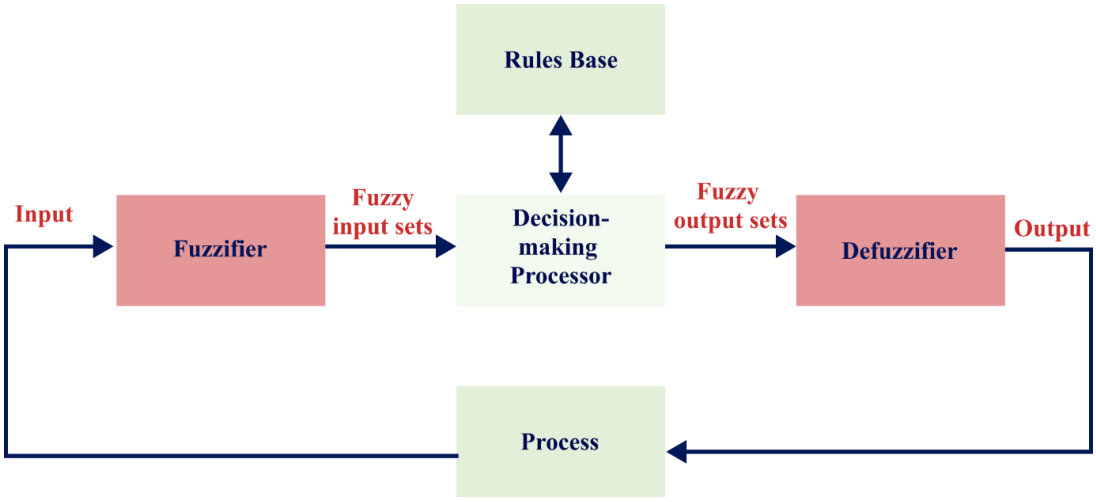

Fig 1. Fuzzy Logic Controller structure

The proposed control design achieves optimized charging of the Lithium-ion battery (LIB), leveraging its chemical capabilities while protecting the battery from overheating and providing early warning about critical health states. This study adopted a quantitative simulation-based research design. This approach is appropriate because the work focuses on testing and validating an improved intelligent charging control algorithm for a Battery Management System (BMS). The design involves modelling battery cells, applying fuzzy logic–based control, and comparing performance metrics (such as thermal stability, energy efficiency, and charging time) against conventional control methods.

The population of interest is rechargeable lithium-ion batteries, which are widely used in electric vehicles (EVs), renewable energy storage systems, and consumer electronics. For practical purposes, this study models a Molicel INR–21700–P45B lithium-ion cell configured in MATLAB/Simulink. This design is suitable because it allows for controlled simulation of thermal stress and aging, direct measurement of system-level performance (temperature rise, current regulation), and verification of the effectiveness of fuzzy logic in improving charging safety compared to traditional methods.

The methodology integrates Battery Modelling (using a Second-Order ECM of the Molicel INR-21700-P45B lithium-ion cell in MATLAB/Simulink), Control Strategy (implementing fuzzy logic controllers for current regulation), Simulation & Validation (MATLAB/Simulink simulations comparing Fuzzy Charging vs. Standard Charging), and Quantitative Analysis (evaluation based on response smoothness, charging speed, power loss, and thermal safety).

3.2.1. Equivalent Circuit Model of Battery

To simulate realistic battery behaviour, a mathematical model representing the internal electrochemical dynamics is required. This study utilizes an Equivalent Circuit Model (ECM) because of its balance between computational efficiency and accuracy.

3.2.2. Basic Model Structure

The basic model consists of an internal resistance. R_o in series with an open circuit voltage source V_{OC}. The terminal voltage equation is expressed as:

$V_{OC} = V_O - V_{RO}$ .....(1)

$V_{RO} = I_b R_o$ .....(2)

Where I_b is the battery current, positive during charging and negative during discharging.

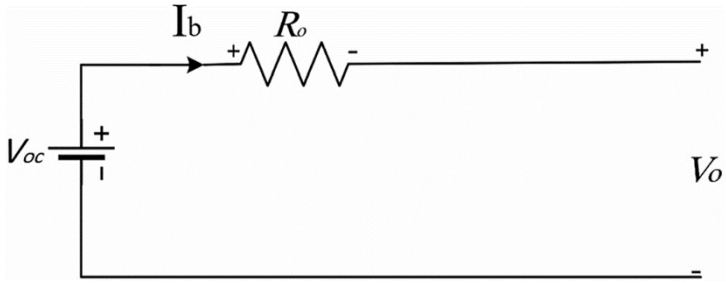

Fig. 2 Basic model of LIB

3.2.2.1. Second-Order ECM Selection

While first-order models are simple, they fail to capture the transient polarisation effects critical for accurate high current charging current control. Therefore, this study employs a Second-Order ECM as illustrated in Fig. 3

Fig 3 presents the configuration of the second-order model, which consists of the following: The Open-Circuit Voltage source (V_{oc}), an internal Ohmic resistance (R_o), and two RC branches connected in series.

The first RC branch ($R_{p1}\|C_{p1}$) represents electrochemical polarisation, while the second branch ($R_{p2}\|C_{p2}$) represents slower concentration polarisation.

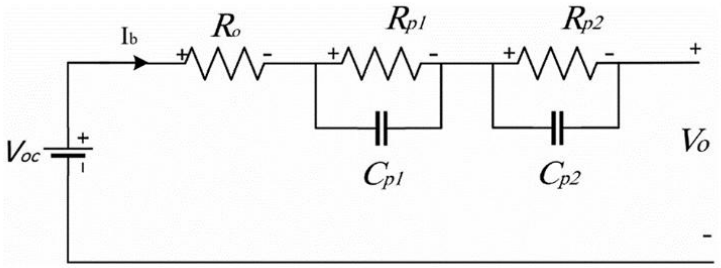

Fig. 3 Second-order LIB equivalent model

Since this study focuses on the charging process, the terminal voltage (V_t)represents the voltage required to overcome the battery's internal potential and impedance. It is governed by the following equation:

$$\boldsymbol{V_t = V_{oc}(SOC) + I_b R_o + V_{p1} + V_{p2}} \quad \text{.....(3)}$$

Where $\boldsymbol{V_{R0} = I_b R_0}$

To model this in a discrete-time domain required for MATLAB/Simulink simulations, the voltage dynamics across each RC branch are calculated at each time step (k) using the following discretization.

$$V_{pn}^{k+1} = V_{pn}[k] \, . \, e^{-\frac{\Delta t}{\tau n}} + I_b^k \, . \, R_{pn} \, (1 - e^{-\frac{\Delta t}{\tau n}}) \quad \text{.....(4)}$$

Where,

n = 1, 2 (representing the First and second RC branches)

V_t = Terminal Voltage

V_{pn} = Polarisation voltage

V_{CPn} = Voltage across the Capacitor (of the n-th branch at the previous time step)

R_{Pn} = Polarisation Resistance

e = Euler's number

V_{oc} = Open circuit voltage, which is a function of the state of charge

I_b = Battery Load current

$\boldsymbol{R_0}$ = Ohmic internal resistance

$\boldsymbol{V_{p1}, V_{p2}}$ = Polarisation voltages across the first and second RC branches

$\boldsymbol{R_{pn}, C_{pn}}$ = Polarisation resistance and capacitance for branch n

Δt = Sampling time interval

τn = Time constant for branch n(s), where $\tau_n = R_{pn} . C_{pn}$

3.2.3 Relevant Mathematical Models and Formulas

To ensure rigorous control logic, the following governing equations are integrated into the methodology:

1. State of Charge (SOC) Estimation

   SOC is the primary fuel gauge for the controller, utilized as a key input for the Fuzzy Logic system. It is calculated using the Coulomb Counting method:

   $$SOC(t) = SOC(0) - \frac{1}{C_n}\int_0^t I(\tau)d\tau \quad \text{.....(5)}$$

   Where,

   C_n = the nominal capacity of the battery, and

   $I(\tau)$ = current over time.

   This shows you're grounding your methodology in mathematical modelling.

2. Battery Voltage Dynamics (Shephard Model)

$$V_{bat}(t) = E_0 - K.\frac{Q}{Q - \int Idt} + A.e^{-B.\int Idt} - R.I \quad \text{.....(6)}$$

E_0 = Constant voltage
K = Polarization constant
Q = Maximum battery capacity
R = Internal Resistance
A, B = Exponential zone parameters

This model captures both steady-state and dynamic responses under load.

4. Fuzzy Logic Controller Output

   The fuzzy logic controller processes the error inputs, specifically SOC deviation, SOH, and Temperature, to determine the optimal charging current (I_c). The control action is defined as:

$$u(t) = \frac{\sum_{i=1}^{n} wi.fi(\Delta SOC,\Delta V)}{\sum wi} \quad \text{.....(7)}$$

Where,

f_i = Fuzzy inference rules

w_i = Membership weights.

This enables adaptive control decisions that outperform fixed-threshold methods.

6. State of Health (SOH) Estimation

   SOH is used to adjust the charging aggressiveness for aged batteries. It is defined as the ratio of current usable capacity to nominal capacity:

$$SOH(t) = \frac{C_{actual}(t)}{C_{nominal}} \times 100\% \quad \text{.....(8)}$$

   Where,

   $C_{actual}(t)$ = current usable capacity

   $C_{nominal}$ = rated nominal capacity

   A decline in SOH affects the weighting functions in the fuzzy logic controller, triggering current derating to preserve life

7. Equivalent Circuit Model (ECM) Voltage Response

   The two-RC or Thevenin model for Li-ion cells:

$$Vcell(t) = E_{ocv}(SOC) - I(t)R_0 - V_{RC}(t) \quad \text{.....(9)}$$

   And,

$$\frac{dV_{RC}}{dt} = -\frac{1}{R_1 C_1} V_{RC} + \frac{I(t)}{C_1} \quad \text{.....(10)}$$

   Where,

   E_{ocv} = open circuit voltage,

   $R_0,\ R_1,\ C_1$ = model parameters capturing ohmic and polarization losses

8. Thermal Dynamics Model

   Since a core objective is thermal safety, the simulation calculates the temperature rise based on internal heat generation (I^2R) convection cooling:

$$C_P \frac{dT}{dt} = I^2 R_{int} - hA(T - T_{amb}) \quad \text{.....(11)}$$

   Where;

   C_P = heat capacity,

hA = convective heat transfer,

R_{int} = internal resistance,

T_{amb} = ambient temperature

9. Energy Efficiency

To evaluate the performance of the intelligent charging strategy, the energy efficiency (η) is calculated by comparing the energy stored in the battery to the total energy supplied by the source:

$$\eta_{deg} = \frac{E_{stored}}{E_{supplied}} \times 100\% = \frac{\int V_{batt} \cdot I_{batt} dt}{\int V_{batt} \cdot I_{batt} dt} \text{ x } 100\% \text{.....(12)}$$

Where $E_{loss,deg}$ represents degradation-induced losses.

Where L and R_L are the inductor and the resistance of the balancing circuits.

3.2.4. Flowchart of Research Design

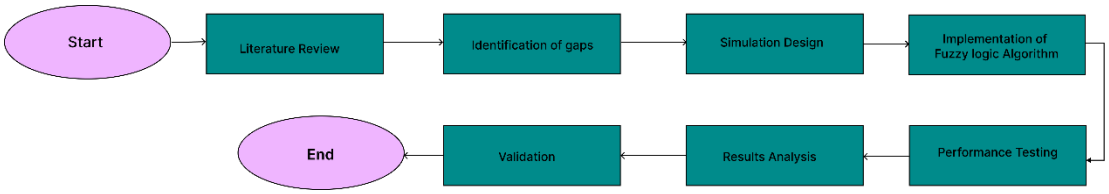

Fig 4. Flowchart for Research Design

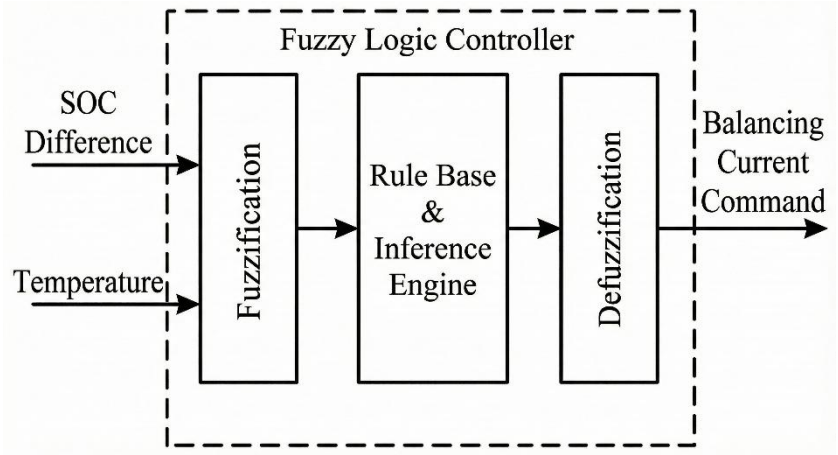

Fig 5. Fuzzy specific diagram

3.2.4.1. Research Population and Sampling

The general population of interest comprises lithium-ion battery systems used in electric vehicles (EVs), renewable energy storage systems, and portable electronics. The sample consists of a representative battery pack model made up of a few series-connected cells, depending on the simulation scope, which provides a realistic yet manageable simulation environment. This sampling choice is justified because a smaller pack allows for computational efficiency while still demonstrating the effectiveness of fuzzy logic in equalising the state of charge across cells. The schematic illustrates a series connection of multiple cells with associated measurement points and balancing circuits.

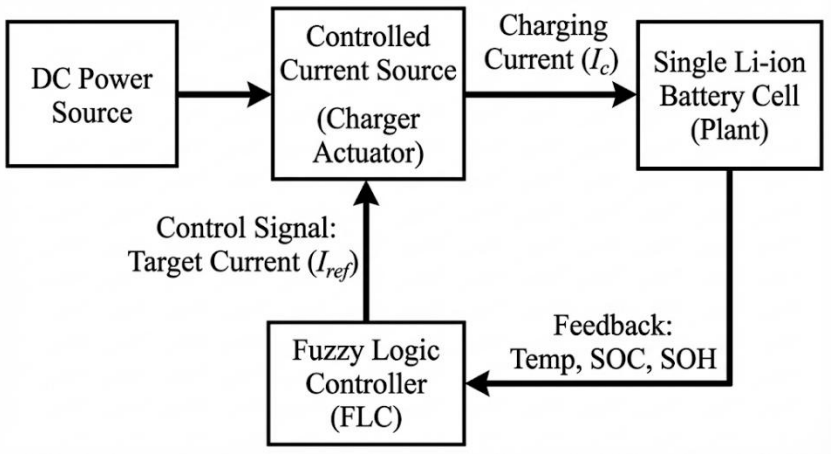

Fig 6. Closed-Loop Feedback Control Architecture for Intelligent Battery Charging

3.3. DATA COLLECTION METHODS

This study relied on simulation-based data collection to evaluate the fuzzy logic–based intelligent charging strategy in a controlled environment. MATLAB/Simulink 2023b, with the Simscape library, was used to model the lithium-ion battery cell, replicate its electrochemical and thermal behaviour, and capture performance data.

3.3.1. Simulation Scenarios

To ensure robustness, the simulation framework incorporated multiple operating scenarios.

Thermal Stress Test: Ambient temperatures were set to 0^{o}C, 25^{o}C, 35^{o}C, 45^{o}C, and 55^{o}C to account for both low-temperature plating risks and high-temperature thermal runaway risks.

Degradation Test: SOH variation from 100% to 90% was included to model cell aging. This tests the controller's ability to "derate" current for older cells.

Full Cycle Test: Charging from 0% to 100% to analyse the transition from Constant Current (Bulk) to Constant Voltage (Saturation).

3.3.2. Data Collection Procedure

The data collection process was organised into two main phases:

Phase 1 (System Design): Input variables (SOC, SOH, Temp) and output variables (Charging Voltage, Charging Current) were defined. Fuzzy linguistic variables (Very Low, Low, Medium, High, Very High) were mapped to these parameters.

Phase 2 (Validation & Benchmarking): The fuzzy controller was evaluated against baseline methods (Triangular MFs vs. Gaussian MFs). Performance metrics recorded included SOC uniformity, Charging Time (time to reach 100% SOC), Voltage Deviation, and Thermal Stability (peak temperature rise).

3.4. SIMULATION CONFIGURATION AND PARAMETER SELECTION

Since this research is simulation-based, the "sample" corresponds to the specific battery cell model and operating conditions chosen for analysis. This study employs purposive sampling to select extreme operating conditions that rigorously test the controller's stability boundaries.

3.4.1. Target Cell Specification

The lithium-ion battery type Molicel INR-21700-P45B was selected as the test cell due to its widespread use in electric vehicles and high-performance energy storage systems [Hameed]. The specifications used for the simulation model are listed in Table. 1

Type	Molicel INR-21700-P45B
Capacity	4,500 mAh
Nominal cell voltage	3.6V
Charge cell voltage	4.2V
Charging current/standard	4.5A or 1C
Charging current/maximum	13.5A or 3C
Charging time	1.5h

Charging temperature	0^{o} C – 60^{o}C
Cut-off charge	70^{o}C
Shape	Cylindrical

Table 1. Battery specifications

3.4.2. Test Scenarios (Sampling Strategy)

To validate the Fuzzy logic controller's robustness, the simulation matrix covers three critical axes of variation.

Thermal Variation: Simulations are conducted at 0°C (Cold), 25°C (Standard), and 55°C (Critical). This selection tests the controller's ability to prevent lithium plating at low temperatures and thermal runaway at high temperatures.

State of Charge (SOC) Sweep: The full range from 0% to 100% SOC is simulated to analyse the transition from Constant Current (Bulk) to Constant Voltage (Saturation) phases.

Degradation States: The controller is tested against a Fresh Cell (100% SOH) and an Aged Cell (95% SOH) to verify that the fuzzy logic correctly derates current as the battery health declines.

3.5. FUZZY LOGIC CONTROLLER DESIGN

The core of this methodology is the Intelligent Fuzzy Controller. This system is designed as a Mamdani-type interference system with three inputs and two outputs.

3.5.1. Fuzzification (Linguistic Variables)

The crisp inputs are mapped to fuzzy linguistic variables: VL, L, M, H, and VH.

SOC input: Determine the charge phase (Bulk vs. Saturation). Range: 0% to 100%.

SOH input: Determines the maximum safe current limit (Derating for age). Range : 0% to 100%.

Temperature input: Acts as a safety throttle. Range: -20^{o}C to 80^{o}C. As shown in Table 2.

	Fuzzy Input			Fuzzy Output	
Rule No.	SOC	SOH	Temp	V_c	I_c
1	VL	VL	VL	VL	VL
2	L	VL	VL	L	VL
3	M	VL	VL	M	VL
4	H	VL	VL	H	VL
5	VH	VL	VL	VH	VL
6	VL	L	VL	VL	VL
7	L	L	VL	L	VL
8	M	L	VL	M	VL
9	H	L	VL	H	VL
10	VH	L	VL	VH	VL
.	.	.	.	.	.
45	VH	H	L	VH	L
46	VL	VH	L	M	H
47	L	VH	L	M	H
48	M	VH	L	H	H
49	H	VH	L	VH	M
50	VH	VH	L	VH	VL
51	VL	VL	M	L	L
52	L	VL	M	L	L
53	M	VL	M	M	L
54	H	VL	M	H	L
55	VH	VL	M	VH	VL
.	.	.	.	.	.
119	H	H	VH	H	L
120	VH	H	VH	VH	VL
121	VL	VH	VH	VL	L
122	L	VH	VH	L	L
123	M	VH	VH	M	L
124	H	VH	VH	H	L
125	VH	VH	VH	VH	VL

Table. 2. FLC Rules

Fuzzy linguistic variables	Inputs Memberships Functions			Output Membership Functions	
	SOC	SOH	Temp	V_C	I_C
VL	SOC < 25%	SOH<10%	Temp < 5^{o}C	2.9V	3.5A
L	SOC < 55%	SOH<30%	Temp < 30^{o}C	3.4V	7A
M	SOC < 70%	SOH<50%	Temp < 50^{o}C	3.9V	10A
H	SOC < 90%	SOH<70%	Temp < 75^{o}C	4.2V	13A
VH	SOC < 100%	SOH<90%	Temp < 80^{o}C	4.3V	16A

Table 3. Description of Fuzzy Linguistic Variables

3.5.2. Membership Function Analysis

A critical aspect of this study is evaluating how the shape of the membership function impacts control smoothness Fig. 7. Two types are modelled and compared:

1. Triangular MFs: Used for baseline testing. These are computationally simple but possess discontinuous derivatives, which can lead to abrupt changes in charging current (chattering). Fig 8a. Ranges for input and output values for Triangular MFs used are listed in Table. 4 & Table. 5.

2. Gaussian MFs: The proposed optimisation. Gaussian functions provide smooth, continuously differentiable control surfaces, theoretically reducing electrical stress on the battery electrodes. Fig. 8b

The specific ranges of input and output values for the Gaussian MFs used in the optimised controller are detailed in Table. 6

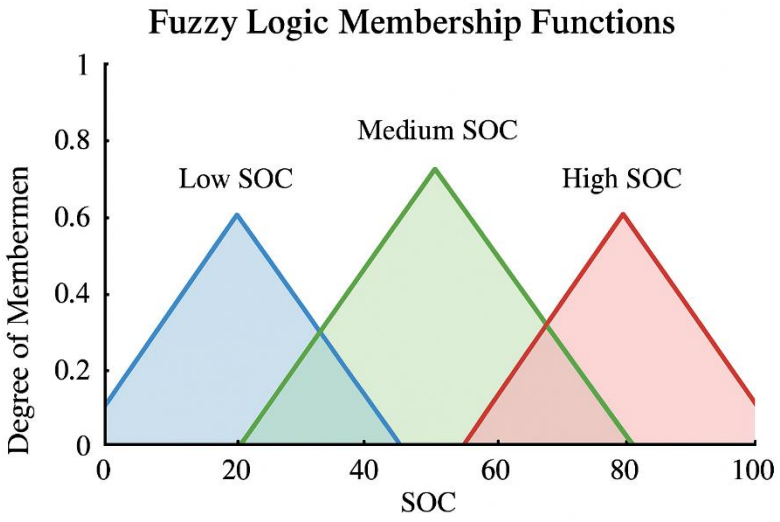

Fig. 7. Fuzzy Logic Membership functions

Fuzzy Linguistic Variables	Range of Inputs		
	SOC	SOH	Temp
VL	[-0.208333 0 0.208333]	[39.5833 50 60.4167]	[-24.5833 -10 4.58333]
L	[0.0416667 0.25 0.458333]	[52.0833 62.5 72.9167]	[-7.08333 7.5 22.0833]
M	[0.291667 0.5 0.708333]	[64.5833 75 85.4167]	[10.4167 25 39.5833]
H	[0.541667 0.75 0.958333]	[77.0833 87.5 97.9167]	[27.9167 42.5 57.0833]
VH	[0.791667 1 1.20833]	[89.5833 100 110.417]	[45.4167 60 74.5833]

Table 4. Ranges of triangular MF of input variables

Fuzzy Linguistic Variables	Range of Inputs	
	V_C	I_C
VL	[2.72917 3 3.27083]	[-5.33333 -2 1.33333]
L	[3.05417 3.325 3.59583]	[-1.33333 2 5.33333]
M	[3.37917 3.65 3.92083]	[2.66667 6 9.33333]
H	[3.70417 3.975 4.24583]	[6.66667 10 13.3333]
VH	[4.02917 4.3 4.57083]	[10.6667 14 17.333]

Table 5. Ranges of triangular MF of output variables

Fuzzy Linguistic Variables	Range of Inputs			Range of Outputs	
	SOC	SOH	Temp	V_C	I_C
VL	[0.08847 0]	[4.424 50]	[6.193 -10]	[0.115 3]	[1.416 -2]
L	[0.08847 0.25]	[4.424 62.5]	[6.193 7.5]	[0.115 3.325]	[1.416 2]
M	[0.08847 0.5]	[4.424 75]	[6.193 25]	[0.115 3.65]	[1.416 6]
H	[0.08847 0.75]	[4.424 87.5]	[6.193 42.5]	[0.115 3.975]	[1.416 10]
VH	[0.08847 1]	[4.424 100]	[6.193 60]	[0.115 4.3]	[1.416 14]

Table 6. Ranges of Gaussian MF for input and output variables

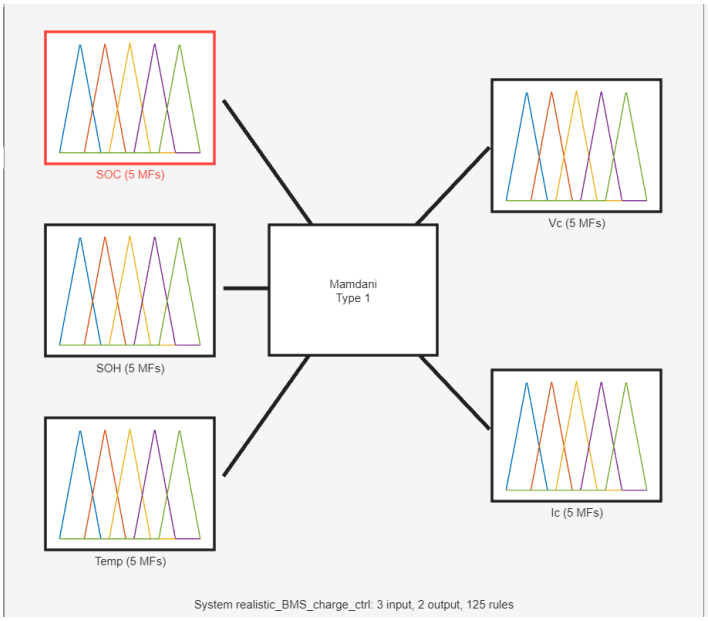

(a)

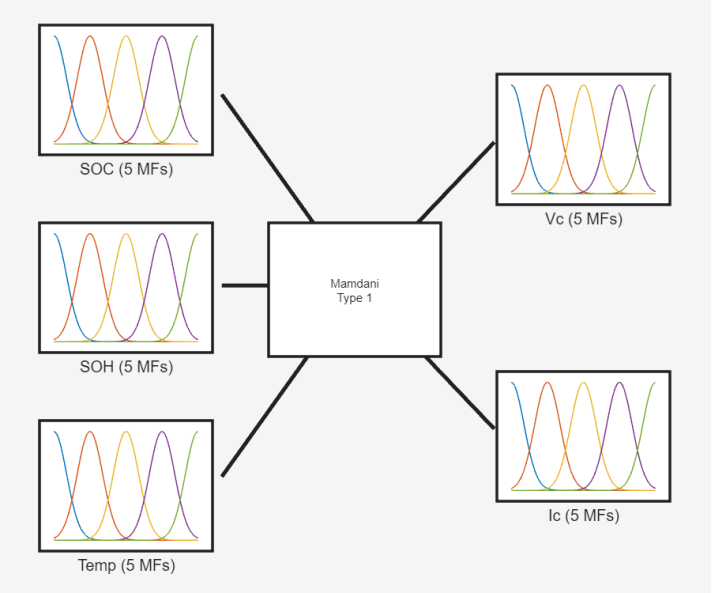

(b)

Fig. 8. Fuzzy Logic for Triangular and Gaussian type variables – (a & b)

3.5.3. Rule Base and Interference

The total number of fuzzy rules is determined by M^N, where M = 5 (number of MFs) and N = 3 (number of inputs), resulting in 125 rules (Table. 2). Examples of the control logic include:

If Temp is High and SOC is High, THEN Current is Low. (Safety Throttling)

If Temp is Medium and SOC is Low, THEN Current is High. (Fast Charging)

3.5.4. Analysis of Control Surface Rules

To visualise the decision-making logic of the controller, Fig. 9 & Fig. 10 illustrate the control surfaces generated by the interference system. The following is illustrated by observing the Gaussian MF Rules relationships control surfaces:

(a) Temperature & Charge Rate Interaction: Charging current is highly sensitive to temperature. The controller permits maximum current injection only within the optimal thermal window (25°C to 45°C). As the temperature rises toward 55°C or drops toward 0°C, the controller automatically throttles the current to minimal levels.

(b) SOC & Voltage Relationship: Charging voltage increases progressively with SOC to match the battery's open-circuit potential, ensuring the cell reaches its 4.2V target without overvoltage.

(c) SOH & Temperature Influence of Current: The interaction between SOH and Temperature is critical for longevity. The controller reduces the charging current for cells with lower SOH (aged cells) or elevated temperatures.

(d) SOH & Temperature Influence on Voltage: SOH and Temperature jointly influence the voltage regulation target to prevent plating or stress under non-ideal conditions.

(e) SOC & SOH Interaction with Charging Current: This surface demonstrates the controller's health-aware derating logic. While low SOC typically triggers high current (bulk charging), the controller automatically scales down this peak current as SOH declines (aged cells). This confirms the system prioritises longevity, sacrificing charging speed on older batteries to minimize internal stress and prevent rapid failure.

(f) SOC & SOH Interaction with Charging Voltage: The voltage regulation is primarily driven by SOC, exhibiting a progressive climb to the 4.2V cut-off to match the Open-Circuit Voltage (OCV). The relative stability of the voltage surface across varying SOH levels indicates that the controller ensures the battery always reaches its full terminal voltage (100% capacity) regardless of health, while the protection is handled entirely by the current throttling in the previous step.

Together, (e) and (f) demonstrate that the controller is smart enough to sacrifice speed (Current) to protect health (SOH) (e), while still guaranteeing a full charge (Voltage) (e).

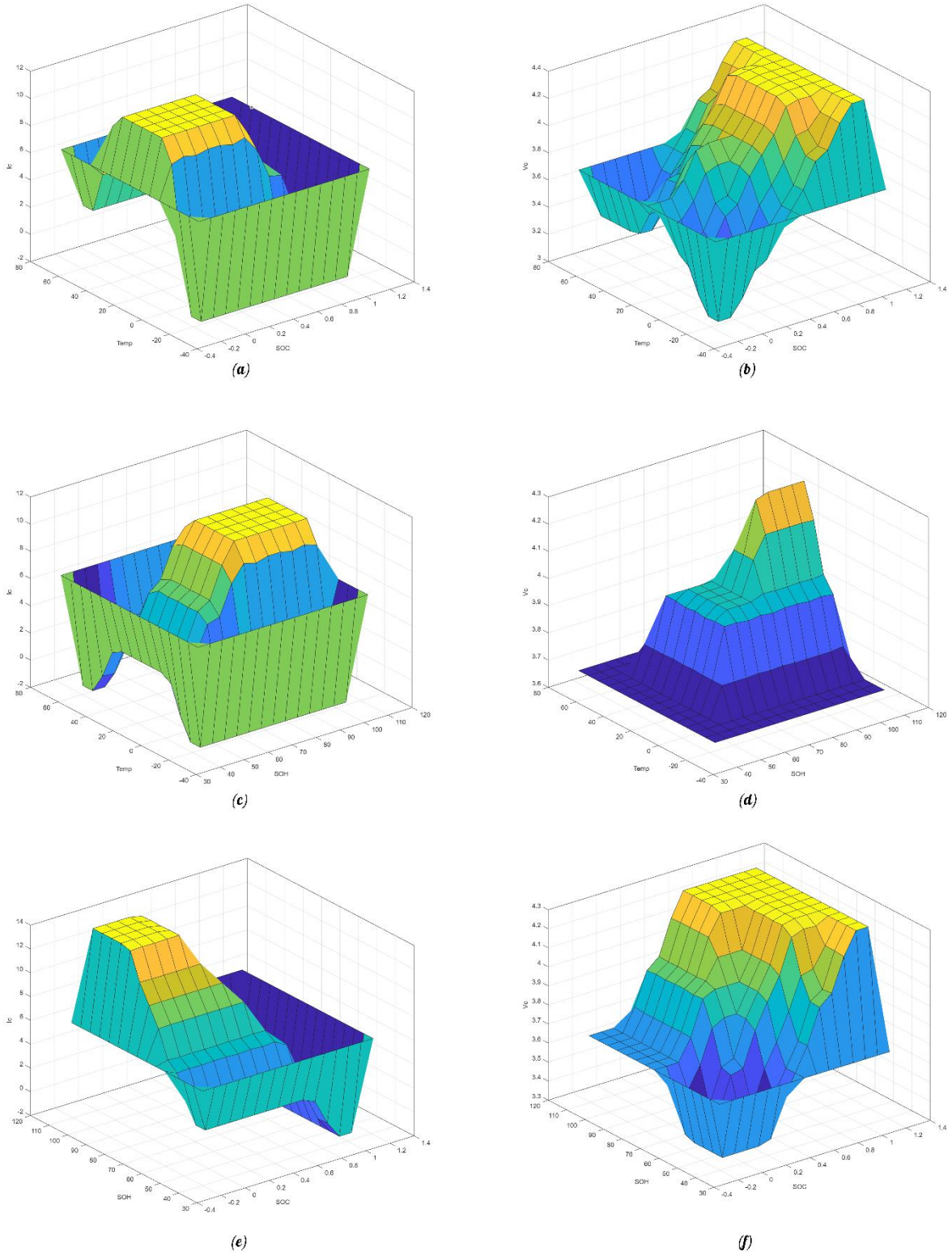

Fig. 9. Triangular MF Rules relationship graphs between (a) SOC and Temp with Charging Current (b) SOC and Temp with Charging Voltage (c) SOH and Temp with Charging Current (d) SOH and Temp with Charging Voltage (e) SOC and SOH with Charging Current (f) SOC and SOH with Charging Voltage

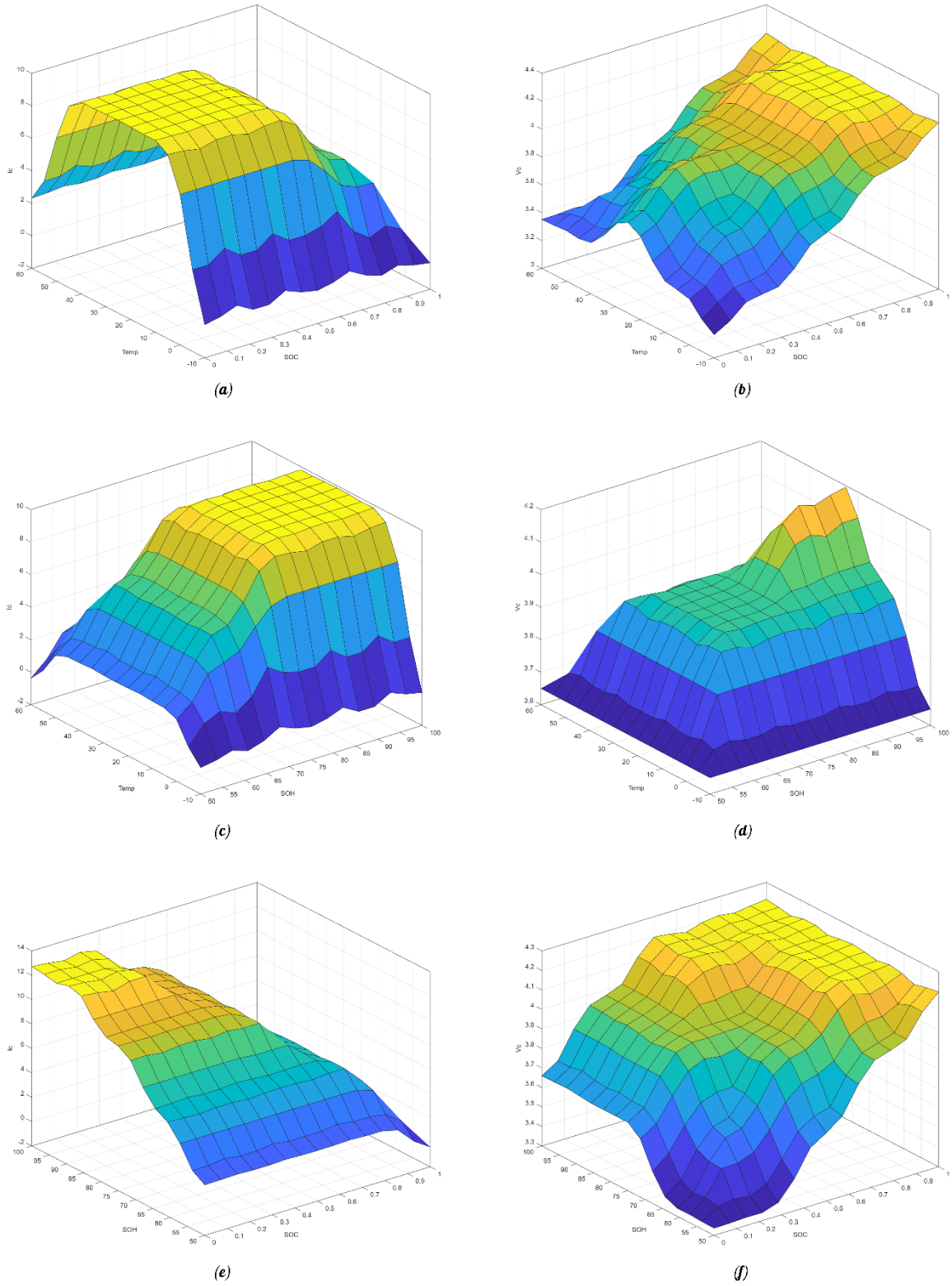

Fig. 10. Gaussian MF Rules relationship graphs between (a) SOC and Temp with Charging Current (b) SOC and Temp with Charging Voltage (c) SOH and Temp with Charging Current (d) SOH and Temp with Charging Voltage (e) SOC and SOH with Charging Current (f) SOC and SOH with Charging Voltage

3.6. SIMULINK MODELLING IMPLEMENTATION

The complete BMS architecture was assembled in the MATLAB/Simulink environment using a combination of Simulink signal and Simscape physical components to reproduce real battery behaviour.

3.6.1. Model Architecture

As shown in the system diagram (Fig. 11), the model comprises of the plant, the controller, and Measurement blocks.

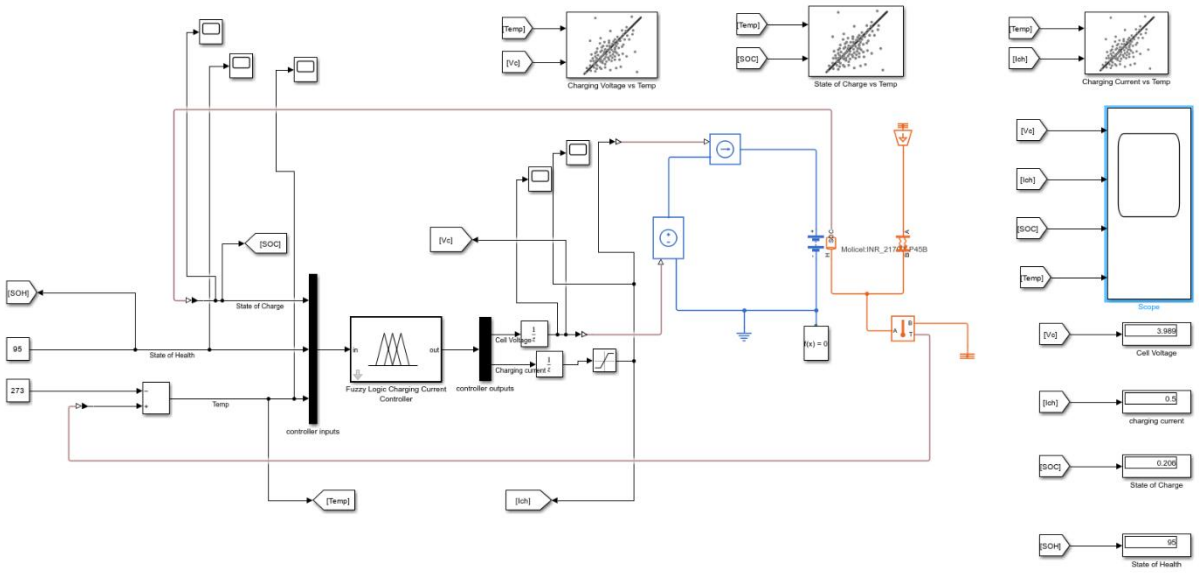

Fig. 11. Simulink of BMS based on environmental effects and thermal mass

3.6.2. Thermal-Electrical Coupling

A critical feature of this methodology is the Thermal Mass subsystem. Thermal interactions are captured by thermal library elements (heat exchangers and thermal ports), enabling heat flow coupling between the electrical and thermal domains. This creates a realistic feedback loop: High current generation leads to High temperature via Joule heating (I^2R). The FLC detects this temperature rise via the feedback sensor. The controller triggers a Reduced Current output to mitigate the thermal runaway.

This closed-loop interaction is essential for validating the system's "Survival Mode", particularly when testing at the critical upper limit of 55°C.

3.7. DATA ANALYSIS TECHNIQUES

In this study, several data analysis techniques were employed to evaluate the effectiveness of the proposed intelligent charging control strategy for the battery management system (BMS).

3.7.1. Data Acquisition and Pre-processing

The analysis began with the acquisition of essential battery state variables, namely State of Charge (SOC), State of Health (SOH), and Temperature, which were obtained from lithium-ion battery models simulated within the MATLAB/Simulink environment (Hameed, Al-Dujaili, & Humaidi, 2025). Since raw sensor and model outputs are often imprecise, pre-processing steps such as normalization and mapping into fuzzy linguistic variables were applied to enable robust interpretation within the fuzzy inference system (Lin et al., 2019).

3.7.2. Model-Based Evaluation

The modelling of battery behaviour was conducted using Equivalent Circuit Models (ECM). A Second-Order ECM was utilized to replicate transient dynamics, polarization effects, and thermal responses, thereby providing realistic data for controller evaluation since it provides higher accuracy than a first-order model (Tran et al., 2021; Baccouche et al., 2021).

3.7.3. Membership Function Comparative Analysis

The Fuzzy Logic Controller (FLC) itself was analysed through its inference process. Two different Membership Function (MF) types, Triangular and Gaussian, were compared to assess their impact on charging performance. Using the Mamdani inference approach, a rule base of 125 rules was generated to map the input conditions into crisp output values (Hameed et al., 2025). Data analysis at this stage focused on evaluating how the choice of membership function influenced accuracy, smoothness of response, and thermal stability during charging operations (Károlyi et al., 2022; Wu & Zhang, 2024).

3.7.4. Key Performance Indicators

To rigorously test the research hypotheses, the collected simulation data were analysed using four key performance indicators:

1. Thermal Stability Analysis: Comparing the temperature rise between Triangular and Gaussian MFs. A lower peak indicated superior safety and reduced risk of thermal runaway. Section 4.2 (4.2.2.1, 4.2.3.1), Section 4.1.2

2. Coulombic Efficiency and Current Stability: Evaluated by analysing the linearity of the SOC rise and the ability to maintain Maximum Current (Coulombic Efficiency). Section 4.2.2.4

3. Rise Time: Time taken to achieve 80% and 100% SOC. Table. 7

4. Response Smoothness: Visual time-domain analysis of the Current (A) vs. Time plots was conducted to identify any harmful oscillations, chattering, or abrupt cut-offs that could degrade battery life. Section 4.1.3, Table. 9, Fig 14 & 15.

5. Comparative Evaluation: The fuzzy controller results are compared against conventional strategies (PID or Standard CC-CV) from other papers to quantify specific improvements in charging time and thermal safety margins. Table. 15

Results indicated that while Triangular membership functions produced sharper but less stable responses, Gaussian membership functions yielded smoother transitions, improved accuracy, and safer thermal management. Chapter 4. (Umair Ali et al., 2018; Hameed et al., 2025).

3.7.5. Comparative Benchmarking against Literature

To validate the proposed approach, a comparative evaluation was conducted against conventional charging strategies, specifically Proportional-Integral-Derivative (PID) control and standard Constant Current–Constant Voltage (CC-CV) charging. Rather than re-simulating these baseline methods, their performance metrics were extracted from verified experimental and simulation studies in the recent literature (Cheng, Lin, & Ho, 2024; Wang et al., 2021). Table. 15. This method facilitated a quantitative assessment of the proposed Gaussian FLC against established industry benchmarks, focusing on key performance indicators such as total charging time and thermal safety margins (Raj et al., 2023; Abdelaal, Mukhopadhyay, & Rehman, 2022).

CHAPTER FOUR – RESULTS

4.1. PRESENTATION OF FINDINGS

Table 7 presents the recorded values of average charging current (Ic) and state of charge (SOC), considering rise times of 80% and 100%, for both types of membership functions (MFs) under various temperature conditions. The sensors monitoring SOC, state of health (SOH), and temperature continuously transmit their respective measurement data on battery states to the fuzzy logic controller (FLC).

States of battery	Temperature				
	0ºC	25ºC	35ºC	45ºC	55ºC
Average charging current controlled using triangular MFs	6.227368	8.362939	8.362939	8.09922	3.82393
Average charging current controlled using Gaussian MFs	5.02225826	7.611008	8.471362	7.89014	4.30027
Rising time of SOC – 80% controlled using triangular MFs	1,480	1,023	1,024	1,125	2,390
Rising time of SOC – 80% controlled using Gaussian MFs	1,519	1,037	1,033	1,192	2,434
Rising time of SOC – 100% controlled using triangular MFs	3,115	2,330	1,731	1,793	3,467
Rising time of SOC – 100% controlled using Gaussian MFs	2,898	1,911	1,720	1,845	3,387

Table 7. Reporting of average charging current and SOC under different ambient temperatures

Figures 12 and 13 illustrate the variation in SOC under different ambient temperatures for controllers based on triangular and Gaussian MFs, respectively. The results indicate noticeable behavioural differences between the two controllers, with their performance metrics summarized in Table 7.

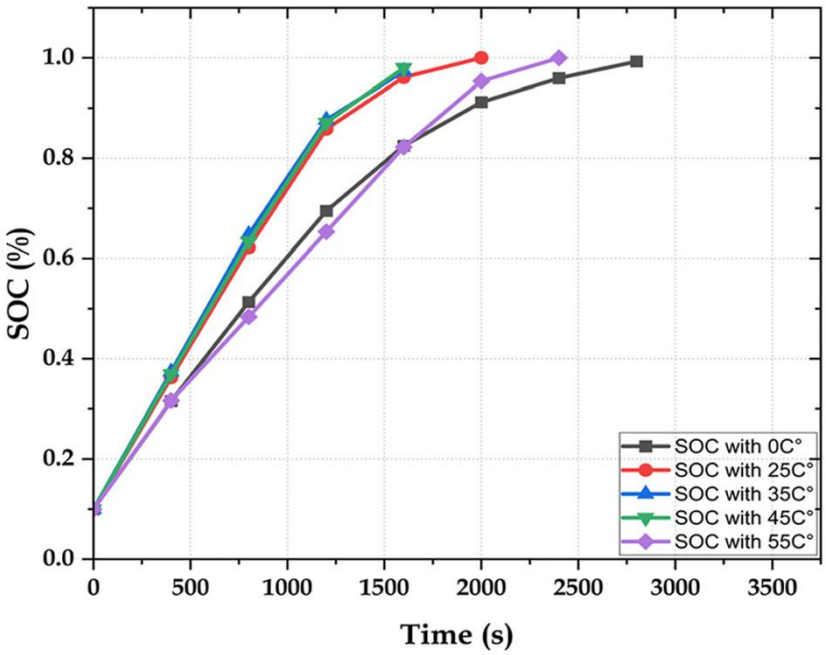

Fig. 12. SOC behaviour under different ambient temperatures controlled using Triangular MF

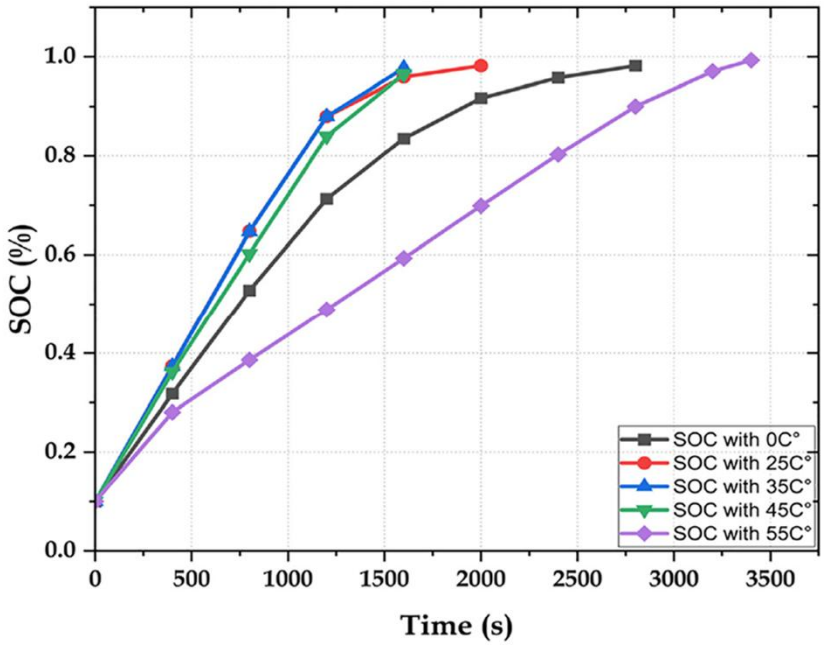

(b)

Fig. 13. SOC behaviour under different ambient temperatures controlled using Gaussian MF

The images present a side-by-side comparison of the State of Charge (SOC) progression under two different Fuzzy Logic MFs. The key finding here is the superior "granularity" and safety of the Gaussian MF, particularly at thermal extremes.

4.1.1. Analysis of Figure 12: Triangular MF

Visual Characteristic: "Clustering" and "Linearity" The Triangular MF produces a control response that is more rigid and distinctively linear. Shown in Fig. 12.

The "Normal" Cluster (25°C, 35°C, 45°C):

The curves for 25°C (Red), 35°C (Blue), and 45°C (Green) are tightly clustered together. They are almost indistinguishable, overlapping significantly throughout the charging cycle. This suggests that the Triangular MF lacks the sensitivity to distinguish fine gradations between "warm" (25°C) and "hot" (45°C) conditions. It treats them all as a generic "Optimal/Standard" state, applying nearly identical current injection rates. All three reach 100% SOC at approximately t = 2,000s.

The Extremes (0°C and 55°C):

0°C (Black): This curve is distinctively slower, reaching full charge at roughly 2,800s.

55 °C (Purple): Interestingly, the triangular controller charges the battery at 55^{o}C faster than at 0^{o}C, reaching completion around 2,400s.

This behaviour at 55^{o}C is potentially risky. By charging faster than the cold scenario, the Triangular controller may not be aggressively throttling enough to prevent thermal runaway.

4.1.2. Analysis of Figure 13: Gaussian MF

Visual Characteristic: "Differentiation" and "Safety Optimisation" The Gaussian MF (which matches the detailed single-graph analyses we did previously) shows a much more nuanced response, separating the temperature cases distinctly. Unlike Fig. 12, the curves in Fig. 13 are clearly separated. The controller is making micro-adjustments based on the specific non-linear properties of the battery at each temperature. The Orange (25^{o}C) and Blue (35^{o}C) curves are the steepest, indicating the highest charging efficiency. They reach full charge fastest, between 1,700s and 1,900s. Notice that the blue curve (35^{o}C) is slightly to the left of the Orange one, confirming 35^{o}C as the absolute optimal electrochemical point. Shown in Fig. 13.

The "safety" Zone (55^{o}C – purple curve): This is the most dramatic difference between the two graphs. In Fig.13, the pink line (55^{o}C) is the lowest and slowest curve by a wide margin. It has a very shallow slope and does not reach full charge until t ≈ 3,400s. The Gaussian controller correctly identifies 55^{o}C as a critical danger zone. Unlike the Triangular controller (which finished at 2,400s), the Gaussian controller throttles the system severely to ensure the battery does not overheat. This proves the Gaussian MF offers superior thermal protection.

The "cold" zone (0^{o}C – brown curve): The brown curve sits in the middle ground, finishing around 3,000s. The Gaussian Controller recognizes that while 0^{o}C is bad (slow kinetics), it is not as immediately catastrophic as 55^{o}C scenario but slower than optimal.

Table 8. Comparative Summary Table

Feature	Triangular MF	Gaussian MF
Response at 25 - 45^{o}C	Clustered / identical behaviour	Distinct / optimised for each temperature.

Response at 55°C (Critical)	Fast (≈ 2,400s). Potentially unsafe	Slowest (≈ 3,400s). Prioritise safety
Control Logic	Linear / Rigid	Non-linear / Adaptive
Overall Verdict	Good for simple control, but lacks precision at extremes.	Superior for BMS applications requiring high safety margins.

The comparison reveals that the Gaussian MF provides superior adaptability compared to the Triangular MF. While the Triangular MF tends to linearise the control output, grouping at 25°C, 35°C, and 45°C responses, the Gaussian MF generates smooth, non-linear control surfaces. Crucially, the Gaussian controller exhibits a "safety first" behaviour at 55 °C, extending the charging duration to 3,400s to mitigate thermal stress, whereas the Triangular controller aggressively charges the cell in just 2,400s, potentially risking thermal runaway.

4.1.3. Comparative Analysis of Membership Function Influence on Controller's Performance

Similarly, Figures 14 & 15 depict the dynamic responses of the charging voltage. V_c, current I_c, SOC, and temperature for FLCs utilizing Triangular and Gaussian MFs. The results clearly demonstrate that the choice of MF has a direct influence on the overall performance of the FLC. The controller employing triangular MFs exhibits relatively sluggish and non-smooth responses, whereas the Gaussian-type MF yields smoother yet slightly slower responses. Therefore, it can be concluded that the FL controller based on the Gaussian-type MF delivers superior performance compared to that using the triangular-type MF.

Accordingly, the Gaussian-type membership function significantly enhances the performance of the Intelligent charging control framework compared to the triangular-type MF when implemented within fuzzy logic controllers. Furthermore, the FLC utilizing a Gaussian MF demonstrates superior accuracy relative to that employing a triangular variant.

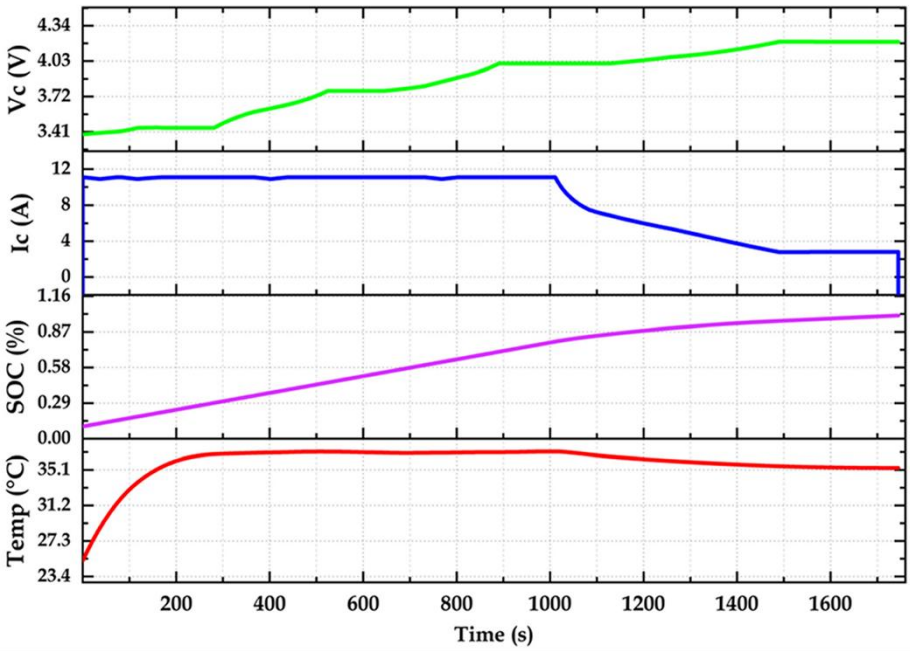

Fig. 14. FLC with Triangular MF

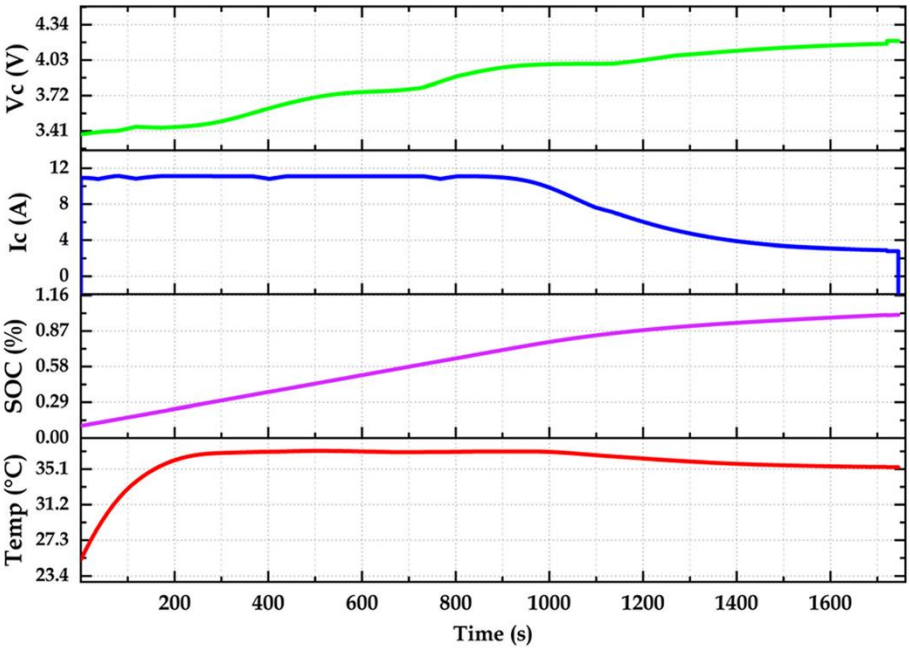

Fig. 15. FLC with Gaussian MF

The technical reasons for these observed differences and the superior performance of the Gaussian MF are evaluated below across four (4) key dimensions:

4.1.3.1. Mathematical Continuity and Derivative Control

Triangular MF (Fig 14): Triangular MFs are piecewise linear functions. While they are continuous (C^o continuity), their first derivative is discontinuous at the peak and base vertices (where the slope changes abruptly from positive to negative or zero). This discontinuity translates into the jagged transitions observed in the I_c and V_c curves. In control terms, this results in abrupt changes in the control gain (dI/dt), creating a "hard-switching" effect as the controller transitions between rules.

Gaussian MF (Fig 15): Gaussian MFs are defined by exponential functions e^{-x^2}, which are continuously differentiable (C^∞ continuity). They possess a smooth, non-zero gradient across their entire domain. The resulting control surface is smooth and devoid of sharp edges (As shown in Fig. 10). The controller modulates current (I_c) with a continuous rate of change, effectively acting as a low-pass filter that rejects high-frequency jitter, yielding the "smoother" response observed in Figure 15.

4.1.3.2. Support and Rule Firing Sensitivity

Triangular (Finite Support): Triangular MFs have “compact support”, meaning the membership grade drops to exactly zero outside a specific interval. If the input variables (SOC, Temperature) fall into a region where rule overlap is minimal (the "valley" between two triangles), the total firing strength of the fuzzy system weakens. This leads to the "sluggish" behaviour where the controller may become unresponsive or seemingly "stuck" until the input state changes significantly enough to trigger the next rule set (Fig. 14).

Gaussian (Infinite Support): Gaussian MFs have “infinite support” (asymptotic behaviour); they never technically reach zero. For any given input state, every rule in the rule base fires to some degree (however small). This global interpolation ensures that the FLC maintains active control authority at all operating points. The controller can "see" trends approaching from a distance, allowing for proactive thermal management rather than reactive switching (Fig. 15).

4.1.3.3. Steady-State Error vs. Transient Response

Triangular Response: The steep slopes of triangular MFs typically provide higher localized gain. This can result in a faster initial rise time (as seen in the sharper initial slope of Fig 14) but often introduces “steady-state chattering”. The controller oscillates

around the setpoint because it lacks the granularity to make fine adjustments without jumping to an adjacent rule.

Gaussian Response: The bell curve shape creates a variable gain, high sensitivity near the centre of the set, and lower sensitivity at the tails. This naturally provides a damping effect, reducing overshoot and oscillation. While this creates a "slightly slower" rise time (overdamped response), it ensures zero-steady-state fluctuation, which is critical for accurate SOC estimation.

4.1.3.4. Electrochemical Stress on the Battery

Stress from Triangular Control: The sharp $^{dI}/_{dt}$ transitions observed in Figure 14 introduce transient current spikes. In Lithium-ion batteries, rapid current fluctuations can cause uneven distribution of lithium ions at the electrode surface (diffusion limitations), potentially accelerating “Solid Electrolyte Interphase (SEI)” layer growth and increasing internal resistance (R_{int}) over time.

Health Benefits of Gaussian Control: The smooth current profile in Figure 15 aligns better with the electrochemical diffusion rates of Li-ions. By avoiding sharp transients, the Gaussian controller minimizes mechanical stress on the electrode lattice, directly contributing to improved State of Health (SOH) retention and cycle life longevity.

While the Triangular MF offers computational efficiency suitable for low-cost microcontrollers, the Gaussian MF provides superior control fidelity. The trade-off of a "slightly slower" response in Figure 15 is technically negligible compared to the benefits of reduced electrochemical stress and improved thermal stability and robustness.

Table 9. Summary of Comparison between Triangular and Gaussian MFs

Technical parameter	Triangular MF (Fig. 14)	Gaussian MF (Fig. 15)
Control Surface	Piecewise Linear (Discontinuous Gradient)	Non-linear curvilinear (continuous gradient)
Rule interaction	Localised / Hard Handoff	Global interpolation / soft handoff
Response characteristic	Fast rise, High Ripple (underdamped)	Slower rise, no ripple (critically damped)

Noise Rejection	Low (Sensitive to sensor noise)	High (intrinsic filtering)
Computational Cost	Low (simple arithmetic operations)	High (requires *exp()* function calculation)

Figures 16–20 below illustrate the variations of charging current (IC), voltage (VC), and state of charge (SOC) under different ambient temperatures: 0°C, 25°C, 35°C, 45°C, and 55°C when controlled by an FL controller based on the Gaussian-type MF. These figures depict the behaviour of power and energy flow into the battery during the charging process. It is observed that I_C and V_C increase proportionally with SOC values below 80%, but exhibit an inverse relationship when SOC exceeds 80%.

4.2. DATA ANALYSIS AND INTERPRETATIONS

4.2.1. Behaviour of charging current, charging voltage, and SOC under 0°C Ambient Conditions

This specific test case highlights a "protective charging strategy". The controller detects the cold environment and actively throttles the system to prevent low-temperature degradation (such as lithium plating). Shown in Fig. 16

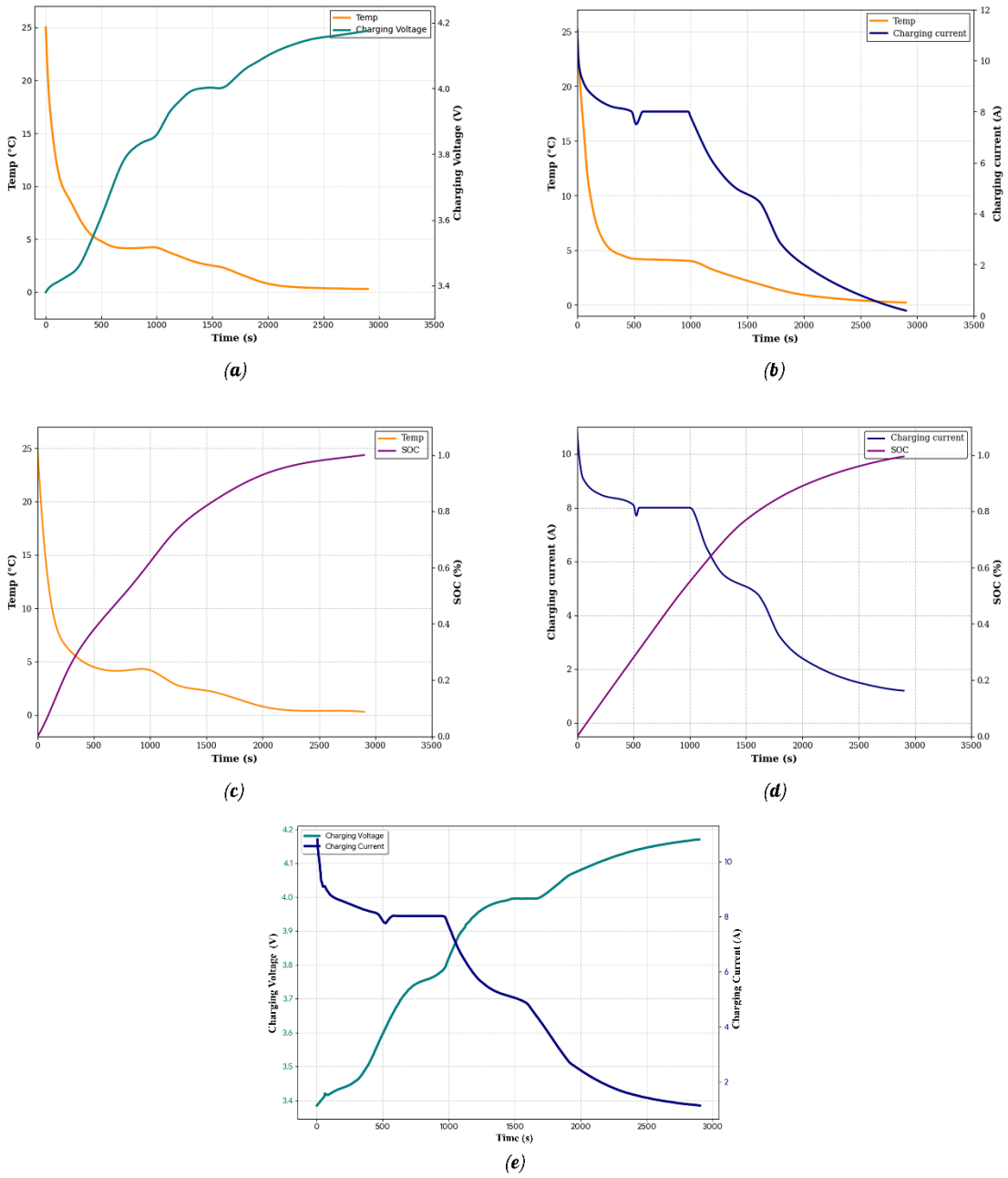

Fig. 16. Behaviour of charging current, charging voltage and SOC under 0°C Ambient conditions

4.2.1.1. Thermal Dynamics (Temperature Analysis)

Observation (Dark orange curve in all subplots, a, b, c)

This 0°C test exhibits a distinct "Cold Soak" thermal profile. The curve does not remain constant at the 0°C ambient setpoint; instead, it illustrates a thermal equilibration

process. The battery is initialized at approximately 25°C (Room Temperature) and rapidly cools down over time, stabilizing near 0°C by the t = 2,500s mark.

This downward trend clarifies that the environmental cooling effect dominates the internal heat generation. Although the charging current generates Joule heating (I^2R) It is insufficient to counteract the convective heat transfer to the freezing 0°C environment. Consequently, the controller is not just managing a static cold battery; it is managing a cooling battery. As the internal temperature drops from 25°C to 0°C, the electrolyte viscosity increases, prompting the controller to reduce power to prevent damage.

4.2.1.2. Charging Current Profile (Current Analysis)

Observation (Navy blue curve in subplots b & d):

The current profile is distinctively "stepped' rather than smooth. At phase 1(0 - 200s), the BMS attempts to start with a high current while the battery is near room temperature (25°C) (≈ 10-11A) but almost immediately throttles it down. Phase 2 (200-1,000s), As the battery temperature drops through approximately 18°C, the controller triggers a protective clamp, reducing the current to a steady plateau of 8A. Crucially, the controller maintains this 8A output even as the temperature continues to slide from ≈ 18°C down to ≈ 4°C (Fig. 16b). This indicates that the Fuzzy Logic controller defines a broad "Cool Zone" (roughly 4°C – 18°C) where 8A is deemed the optimal safe limit. Phase 3 (1,000-1,700s), As the temperature stabilises near freezing (≈ 4°C), the controller crosses a second threshold, forcing a further reduction to 5A to prevent plating at critical low temperatures. At Phase 4 (>1,700s), the system enters the final saturation phase, exponentially decaying towards 0A.

These distinct 'steps' are deliberate control actions reacting to thermal thresholds. As the cell cools, the electrolyte conductivity drops and charge transfer resistance increases. If the controller maintained high current while the temperature dropped, it would cause a voltage spike and potential lithium plating.

The stepped reduction (11A → 8A → 5A) demonstrates a zonal control strategy: once the temperature stabilises near freezing (< 4°C), the system enforces a strict reduction, effectively matching the charge rate to the battery's diminishing capacity to accept ions without degradation.

4.2.1.3. Voltage Response (Voltage Analysis)

Observation (Deep teal curve in subplot a):

The voltage starts at ≈ 3.4V and rises to the 4.2V cut-off. The voltage curve is not a smooth arc; it has visible "wobbles" or inflection points that align perfectly with the current steps. Between t = 1,000s and t = 1,500s, the voltage slope flattens slightly (Fig. 16a). This corresponds to the moments the current drops from 8A to 5A, reducing the ohmic voltage drop ($V_{drop} = I \times R_{internal}$). (Fig 16e)

The voltage hits the 4.2V ceiling around t = 2,500s, which is much later than warmer scenarios (As seen in Fig 17, 18, 19). This delay is due to the reduced current injection rate required to navigate the freezing ambient conditions safely.

4.2.1.4. State of Charge (SOC) Evolution

Observation (Dark purple curve in subplots c & d):

The SOC rises linearly during the 8A constant current phase but begins to curve (slow down) significantly after t = 1,500s (Fig. 16d). Full charge (100% or 1.0 SOC) is achieved at approximately 3,000s.

The charging process is considerably slower here compared to the warmer test cases (which finished in ≈ 1,800s) (Table. 12 & 13).

The "knee point" where the charging slows down happens at a lower SOC (≈ 60%). This indicates that while the battery can accept a bulk charge initially (due to starting at 25^{o}C) (Fig. 16b, 16d), its efficiency degrades rapidly as it approaches thermal equilibrium with the 0^{o}C environment.

Table 10.

Summary Table for 0^{o}C Scenario	
Parameter	Value / Behaviour
Total Charge Time	≈ 3,000s (slow)
Max Sustained Current	≈ 8A (Throttled from 11A)
Thermal Behaviour	Cools from 25^{o}C to 0^{o}C
Key Characteristic	Multi–stage stepped current reduction to prevent plating

4.2.2. Behaviour of charging current, charging voltage, and SOC under 25ºC Ambient Conditions

This scenario represents "standard room temperature operation". The controller balances charging speed with thermal stability, resulting in a distinct "double-peak" thermal signature and highly efficient bulk charging phase. Shown in Fig. 17

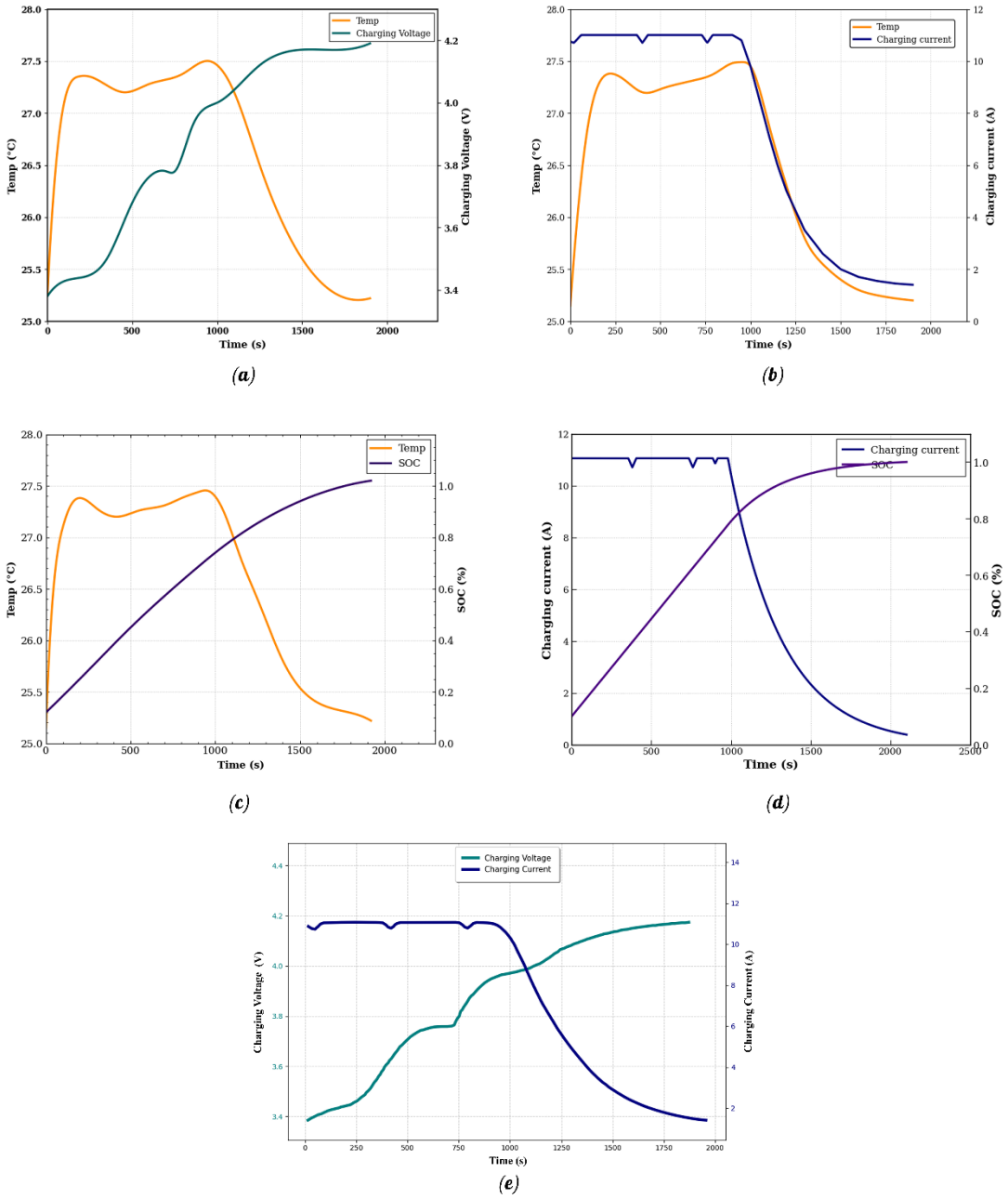

Fig. 17. Behaviour of charging current, charging voltage and SOC under 25 °C ambient conditions

4.2.2.1. Thermal Dynamics (Temperature Analysis)

Observation (Dark orange curve in subplots a, b, c):

Unlike the 0°C scenario where the battery cools down, here the system begins in a state of Thermal Equilibrium: the initial battery temperature (≈ 25°C) is already synchronised with the ambient environment. Within the first 200s, the temperature spikes to a local maximum of ≈ 27.4°C. This indicates that the internal heat generation (I^2R losses) momentarily overcomes the convective cooling capacity of the 25°C environment. Following next is the Intermediate Dip. Between 200s and 600s, the temperature stabilises and dips slightly to ≈ 27.2°C. This "dip" is physically significant: as the cell warms up, the electrolyte viscosity decreases, and ionic conductivity improves, causing a temporary reduction in internal resistance. Consequently, the rate of heat generation drops slightly below the rate of convective cooling, leading to this cooling valley. The Second Rise (Peak), here, as the battery approaches the end of the constant current phase (t ≈ 1,000s), the temperature rises again to its absolute peak of 27.5°C (Fig. 17a). Lastly, the Cooling Phase, once the current tapering begins (after 1,000s), the temperature drops rapidly, returning the near ambient levels (25.2°C) by the end of the cycle. (Fig. 17b).

The "double-peak" profile is characteristic of reactive thermal management at moderate temperatures. This peak temperature rise is small (< 2.5°C total increase), confirming that 25°C is a thermally safe operating zone that requires minimal throttling.

The 25°C ambient temperature acts as a thermal stabiliser. Unlike the freezing case, the 25°C air allows the battery to operate naturally, absorbing the minor waste heat (<2.5°C) and restoring equilibrium quickly after the bulk phase.

4.2.2.2. Charging Current Profile (Current Analysis)

Observation (Navy blue curve in subplots b & d):

Starting with the bulk phase (0 – 1,000s): The controller maintains a high, stable current of approximately 11A. In the Micro-Adjustments phase, notice the small "notches" or dips in the current plateau (visible at t ≈ 400s and t ≈ 780s in the subplot Fig. 17b). These are momentary checks by the Fuzzy Logic Controller to assess internal resistance or thermal feedback without disrupting the main charge flow. Tapering phase (1,000s – 1,900s): At t ≈ 1,000s, the current transitions into an exponential decay (Fig. 17b). Unlike the step-down seen at 0°C (Fig. 16b, 16d), this is a smooth, continuous drop

consistent with standard Constant Voltage (CV) charging dynamics. At the termination, the current reaches the cut-off threshold (≈ 1.5A) at t ≈ 1,900s.

The ability to hold 11A for over 50% of the cycle duration allows for rapid capacity recovery. The smooth transition at 1,000s indicates the battery reached its voltage ceiling without hitting any thermal safety limits that would force a premature abort.

4.2.2.3. Voltage Response (Voltage Analysis)

Observation (Deep teal curve in subplot a):

The voltage starts at ≈ 3.4V and rises monotonically (Fig. 17a). At the Inflection point, there is a distinct "knee" or steepening of the slope at t ≈ 800s (voltage rising from 3.8V to 4.0V). This corresponds to the final stage of the bulk charging phase, where the cell's internal resistance often changes as ion intercalation saturates the anode. Saturation, the voltage hits the 4.2V limit at approximately 1,600s and holds steady.

The voltage curve is significantly smoother than the multi-stepped profile seen in the 0^{o}C scenario (Fig. 16a). It rises monotonically with stable kinetics, interrupted only by a minor inflection at t ≈ 750s. This transient voltage dip corresponds to the momentary current 'notch' (Fig. 17e) where the controller performed a resistance check, further confirming the direct correlation between the input current regulation and the voltage response.

4.2.2.4. State of Charge (SOC) Evolution

Observation (Dark purple curve in subplots c & d):

At first, the Linear growth, the SOC increases linearly from 0 to ≈ 0.8 (80%) during the first 1,000s. This linearity confirms that the charging efficiency (Coulombic efficiency) is high during the constant current phase (Fig. 17b, 17c). After 1,000s, the slope flattens as the current drops. In the completion stage, the battery reaches 100% SOC (1.0) at roughly 1,900s.

This 1,900s charge time is significantly faster than the cold weather scenario (3,000s) but slightly slower than the optimal 35^{o}C scenario (1,700s) in Fig. 18, suggesting that while 25^{o}C is standard, it is not the peak efficiency point for this specific chemistry.

Table 11.

Summary Table for 25°C Scenario	
Parameter	Value / Behaviour
Total Charge Time	≈ 1,900s (standard)
Max Sustained Current	≈ 11 A (High stability)
Thermal Behaviour	"Double Peak" rise: 25.2°C to 27.5°C
Key Characteristic	Stable bulk charging with minimal thermal stress (ΔT < 2.5°C)

4.2.3. Behaviour of charging current, charging voltage, and SOC under 35°C Ambient Conditions

This scenario represents the "optimal operating condition" for the battery charging system. The Fuzzy Logic Controller achieves the fastest charging time with the most stable thermal profile, indicating peak electrochemical efficiency. Shown in Fig. 18.

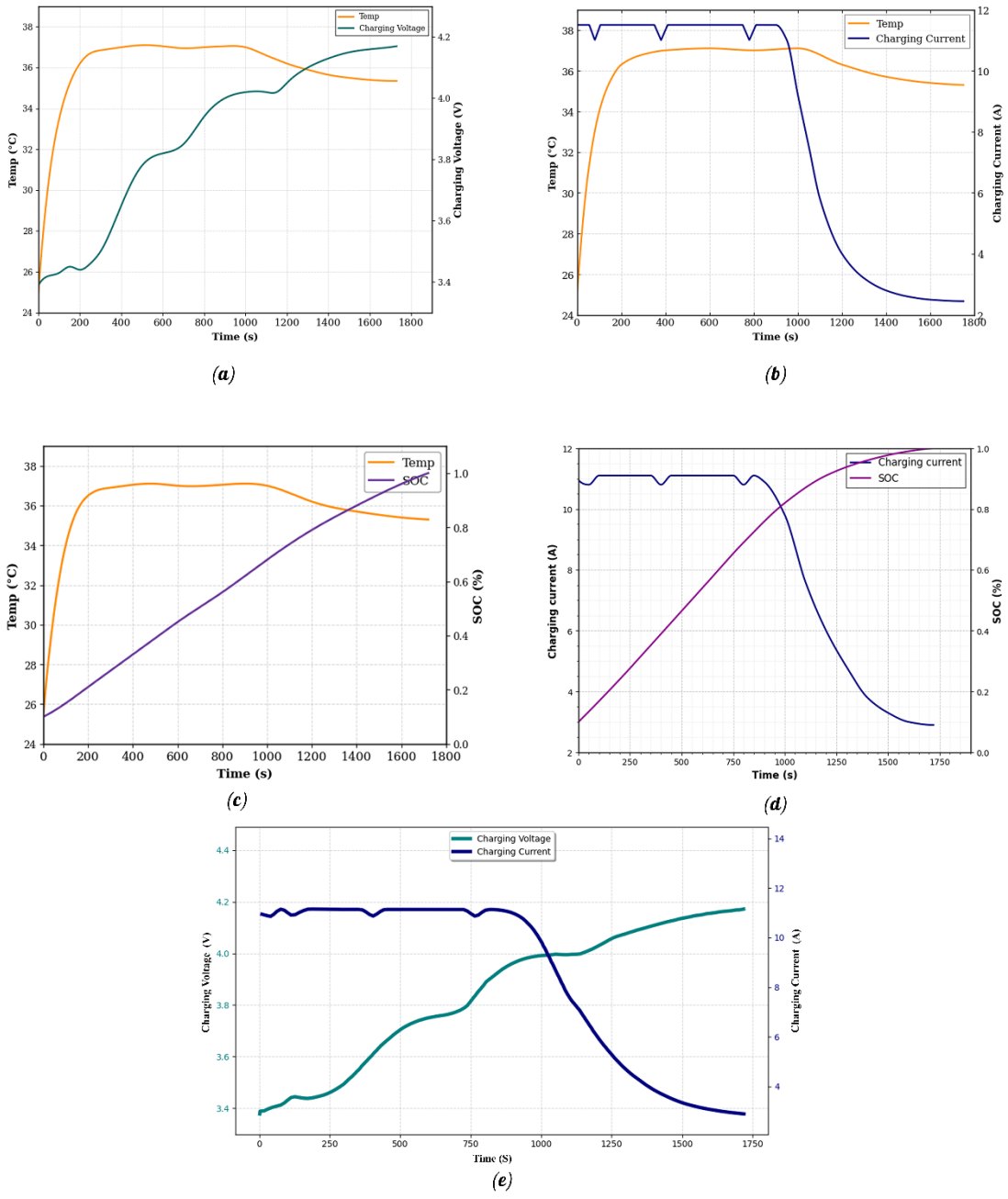

Fig. 18. Behaviour of charging current, charging voltage, and SOC under 35°C ambient conditions

4.2.3.1. Thermal Dynamics (Temperature Analysis)

Observation (Dark orange curve in subplots a, b, c):

The battery initialises at the ambient temperature of approximately 25°C (indicating the initial cell temperature before self-heating) and rises steeply within the first 200s to

settle near 36.5°C. Unlike the "double peak" seen at 25°C (Fig. 17), the temperature here forms a nearly flat, perfect plateau between 36.5°C and 37°C from t = 400s to t = 1,000s. This indicates a perfect balance between heat generation (I^2R losses) and dissipation. After t = 1,000s, as the charging current drops, the temperature decays smoothly, ending at approximately 35.5°C (Fig. 18b).

The stability of the temperature curve (lack of significant fluctuations) confirms that 35°C facilitates optimal ion transport, minimising internal resistance and excess heat generation (as opposed to the double peak rise of temp. at 25°C Fig. 17a, ambient temperature).

4.2.3.2. Charging Current Profile (Current Analysis)

Observation (Blue curve in subplots b & d):

In the bulk phase (0 – 900s), the controller sustains the maximum charging current of 11 A for a prolonged duration. There are visible oscillations or "ripples" in the current plateau (seen clearly in subplot Fig. 18b). These are characteristic of the Fuzzy Logic Controller constantly tuning the current to maintain the edge of the safe operating area without crossing it. The transition from Constant Current to Constant Voltage occurs at t ≈ 1,050s (Fig. 18e). As validated in Fig. 18c, d, this cut-off is triggered precisely when the SOC breaches the 80% threshold, causing the controller to shift priority from speed to saturation. The charging process completes (current drops to cutoff) at approximately 1,750s.

This is the fastest charging cycle across all datasets. The ability to sustain 11A for nearly 60% of the cycle results in rapid SOC gain.

4.2.3.3. Voltage Response (Voltage Analysis)

Observation (Deep teal curve in subplot a):

The voltage curve exhibits a unique "staircase" or stepped behaviour during the bulk phase. Phase 1, the initial fluctuation and rise to 3.5V in 250s, featuring a visible dip at t ≈ 150s. Followed by steady ascent crossing 3.6V at t ≈ 400s. Sharp rise through 3.8V from 600-700s. Last phase shows a distinct plateau at ≈ 4.0V (1,000-1,150s) before the final smooth approach to saturation (Fig. 18a, 18e).

These voltage steps likely correspond to phase transitions within the battery's electrode materials (intercalation stages). At 35^{o}C, the kinetics are sufficiently fast that these electrochemical stages become distinct and visible in the voltage response.

4.2.3.4. State of Charge (SOC) Evolution

Observation (Dark purple curve in subplots c & d):

Initially, Rapid Linearity is exhibited. The SOC climbs from 0.1 (10%) to 0.9 (90%) with a steep linear slope. The Linearity is maintained up to a higher SOC threshold compared to the colder scenarios (Fig. 16c, 16d). The battery reaches 100% SOC at ≈ 1,700s.

The steepness of the SOC curve indicates that this ambient temperature yields the highest coulombic efficiency.

Table 12.

Summary Table for 35^{o}C Scenario	
Parameter	Value / Behaviour
Total Charge Time	≈ 1,700s (Fastest / Optimal)
Max Sustained Current	≈ 11 A (Held for 900s)
Thermal Behaviour	majorly stable plateau at ≈37^{O}C
Key Characteristic	Peak efficiency; fastest charging with minimal thermal stress

4.2.4. Behaviour of charging current, charging voltage, and SOC under 45^{o}C Ambient Conditions

This scenario represents a "High Temperature operation". While the charging speed remains competitive, the data reveals that the controller is actively intervening (throttling) to prevent the battery from crossing thermal safety thresholds, evidenced by the unstable current plateau. Shown in Fig. 19.

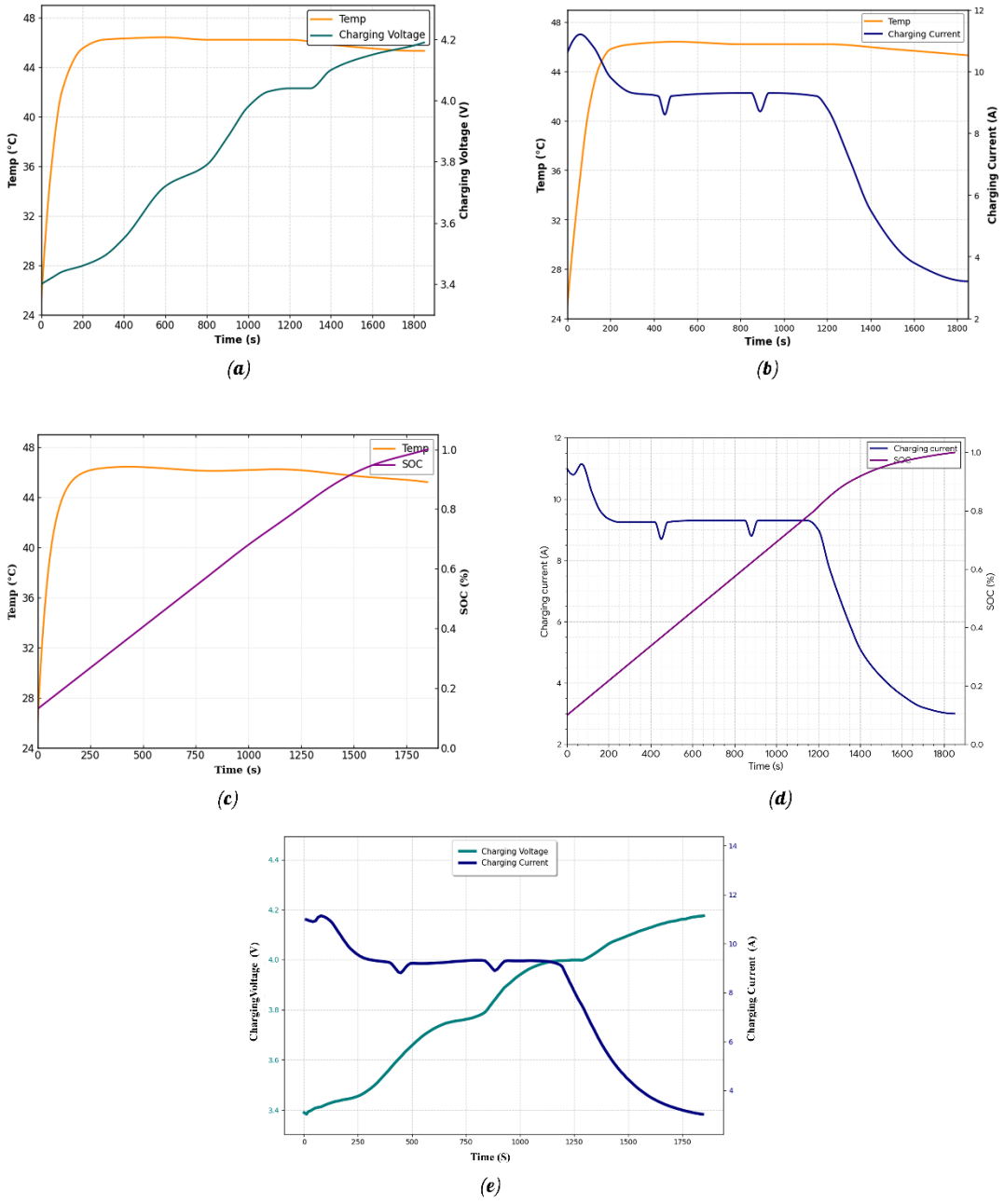

Fig. 19. Behaviour of charging current, charging voltage and SOC under 45°C Ambient condition

4.2.4.1. Thermal Dynamics (Temperature Analysis)

Observation (Dark orange curve in subplots a, b, c):

Firstly, Rapid Acclimatization. The battery starts at room temperature (≈ 26°C) and undergoes a massive temperature rise, shooting up to ≈ 46°C within the first 300s (Fig.

19a). The 20°C delta is driven by the ambient environment combined with internal joule heat. Unlike the "cooling" seen at 0°C (Fig. 16) or the "gentle" rise at 35°C (Fig. 18), the temperature here rapidly hits a "soft ceiling". It saturates and holds a high steady state between 46°C and 46.5°C for the majority of the cycle (300s to 1,400s). The peak roughly touches 46.5°C. This is dangerously close to common degradation thresholds (50 °C+). The flat, non-increasing nature of the curve suggests the controller is modulating power specifically to keep the temperature from exceeding the 47°C ceiling.

4.2.4.2. Charging Current Profile (Current Analysis)

Observation (Navy blue curve in subplots b & d):

Instability/Derating, this is the defining characteristic of the 45°C graph. The controller attempts to reach the maximum 11A (seen at t = 100s), but cannot sustain it (Fig. 19b). Following this, we see the Throttled Plateau, instead of a flat line at 11A (as seen at 35°C), the current drops to a fluctuating plateau averaging around 9.2A (Fig. 19b, 19d, 19e). There are two distinct "dips" or notches in the current profile: At t ≈ 450s, current dips to ≈ 8.8A. At t ≈ 880s, current dips again to ≈ 8.8A. These dips are not random; they coincide perfectly with the voltage inflection points (Fig. 19e). This confirms Closed-Loop Control: the controller detects a rise in internal resistance or temperature flux and momentarily backs off the current to stabilise the system before ramping back up.

4.2.4.3. Voltage Response (Voltage Analysis)

Observation (Deep teal curve in subplot a):

The "stepped" behaviour is most pronounced in this 45°C scenario. Step 1: Rapid rise to 3.4V (0 – 200s). Step 2: Slower rise to 3.8V (200 – 900s), featuring an inflection point at t = 500s. Step 3: Sharp rise to 4.1V (900 – 1,200s). The "wobble" in the voltage curve at t = 450s and t = 880s align perfectly with the current throttling events (Fig. 19e). This confirms that the BMS is reacting to voltage feedback loops that are more volatile at high temperatures.

4.2.4.4. State of Charge (SOC) Evolution

Observation (Dark purple curve in subplots c & d):

The SOC rise is linear but slightly less steep than the 35ºC graph due to the current being throttled from 11A down to ≈ 9.2A. Full charge is reached at approximately 1,850s.

While 45ºC is a high-stress environment, the charging time (1,850s) is still very competitive with the optimal 35ºC time (1,700s) (Table. 12). This proves the FL controller successfully executes a Safety Speed Trade-off: it sacrifices a small amount of speed (150s delay) to ensure thermal safety.

Table 13.

Summary Table for 45ºC Scenario	
Parameter	Value / Behaviour
Total Charge Time	≈ 1,850s (Fast, buy throttled)
Max Sustained Current	≈ 9.2 A (Derated from 11A target)
Thermal Behaviour	Rapid saturation at 46.5ºC
Key Characteristic	Visible current oscillation ("Dips") to manage high heat.

4.2.5. Behaviour of charging current, charging voltage, and SOC under 55ºC Ambient Conditions

This scenario represents a "Critical Thermal Operation". This data clearly demonstrates that the Fuzzy Logic Controller has entered a "Survival Mode", aggressively sacrificing charging speed to maintain physical safety and prevent thermal runaway. Shown in Fig. 20.

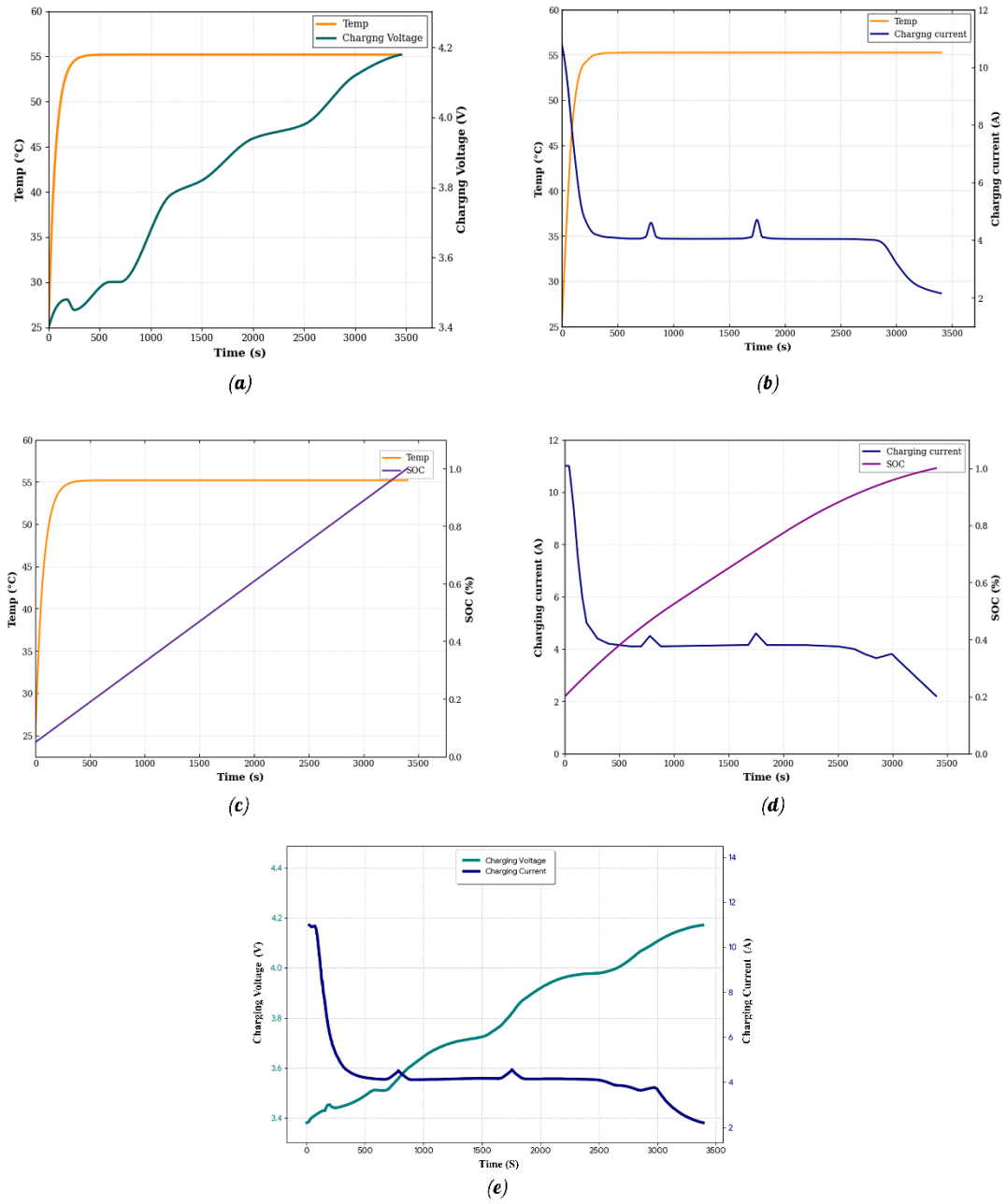

Fig. 20. Behaviour of charging current, charging voltage and SOC under 55 °C ambient conditions

4.2.5.1. Thermal Dynamics (Temperature Analysis)

Observation (Dark orange in subplots a, b, c):

The temperature profile is drastic. The cell temperature rockets from an initial ≈ 26ºC to the ambient ceiling of 55ºC within the first 300s (Fig. 20a). While the initial burst of

current adds some internal heat, this rapid rise is primarily driven by the massive thermal gradient (55^{o}C - 26^{o}C = 29^{o}C). The battery is essentially undergoing “Heat Soak” from the hot environment. The initial 11A current acts as a catalyst, accelerating the rise, but the trajectory towards 55^{o}C is inevitable due to the environmental conditions. (Fig. 20b)

Once it hits 55^{o}C, the curve flatlines perfectly. It maintains a constant temperature of ≈ 55.2^{o}C for the entire duration of the charge (from t = 300s to t = 3,400s). The temperature does not significantly exceed 55^{o}C confirming that the controller has reduced the current (4A) to a point where internal heat generation is negligible, allowing the battery to simply exist in equilibrium with the hot environment.

4.2.5.2. Charging Current Profile (Current Analysis)

Observation (Navy blue in subplots b & d):

This is the most significant feature. At t = 0s, the controller attempts to inject the standard 11A, but within 200s, the current crashes vertically down to ≈ 4A. Unlike the 11A sustained at optimal temperatures (Fig. 17, 18), the system holds a very low steady state of ≈ 4.1A for nearly 2,500s (from t = 500s to t = 3,000s). This 4A level represents the maximum safe current that generates minimal joule heating, ensuring the cell temperature (≈ 55^{o}c) does not rise further above the ambient floor.

Small “blips” are visible at t ≈ 750s and t ≈ 1,750s (Fig. 20b). That is the controller briefly testing if it can increase current, detecting thermal resistance, and immediately clamping it back down.

This behaviour represents a massive ≈ 63% derating in charging power (from 11A down to 4A). The BMS has determined that 11A would cause the battery to overheat beyond 55^{o}C, so it forces a slow, trickle-like charge to maintain safety.

4.2.5.3. Voltage Response (Voltage Analysis)

Observation (Deep teal curve in subplot a):

A pronounced staircase, the voltage curve is extremely “stepped”, more so than any other scenario (Fig. 16 - 19). The charging voltage curve shows an initial rise to ≈ 3.45V (0 – 200s), interrupted by a distinct dip at t ≈ 200s, after which a clear plateau/shallow rise near 3.5V is visible between 500s and 700s. This is followed by a sharp rise,

transitioning into a significant plateau region around 3.8V from 1,200s to 1,500s, and then a final ascent toward the 4.2V saturation limit, which it approaches smoothly after 3,000s.

These distinct steps are visible because of the low charging current (4A). When charging current is low (low C-rate), the voltage curve closely follows the battery's Open Circuit Voltage (OCV) profile, revealing the electrochemical phase transitions of the electrode materials that are usually smoothed out at high currents (Fig. 20e)

4.2.5.4. State of Charge (SOC) Evolution

Observation (Dark purple curve in subplots c & d):

This SOC slope is linear but very shallow. It rises much more slowly than in 35^{o}C or 25^{o}C cases. Exhibiting Extended Duration, the battery finally reaches 100% (SOC) at approximately 3,400s. This is the longest charging duration observed (even longer than the freezing 0^{o}C scenario). It confirms that high-heat protection is the most restrictive constraint in this control logic. To prevent thermal runaway in a 55^{o}C environment, the controller must sacrifice speed entirely, accepting a 2× increase in charge time to ensure physical safety (Fig. 20c, 20d)

Table. 14.

Summary Table for 55^{o}C Scenario	
Parameter	Value / Behaviour
Total Charge Time	≈ 3,400s (Slowest / Safest)
Max Sustained Current	≈ 4 A (Severely throttled)
Thermal Behaviour	Immediate saturation at 55^{O}C
Key Characteristic	"Survival Mode" – 63% current reduction to prevent runaway (Fig. 20e)

The proposed BMS employs an FL controller to optimize battery power utilization during specific charging cycles. Figures 16–20 present the charging profiles of the battery under various ambient temperatures at a state of health (SOH) level of 95%. As evident from the figures, the charging current remains constrained by the current specifications provided in Table 4.

4.3. COMPARATIVE ANALYSIS OF CONTROL TRIGGERS: SOC-DOMINANT TRANSITION (35ºC) – OPTIMAL, VERSUS THERMALLY-DOMINANT INTERVENTION (55ºC) – CRITICAL.

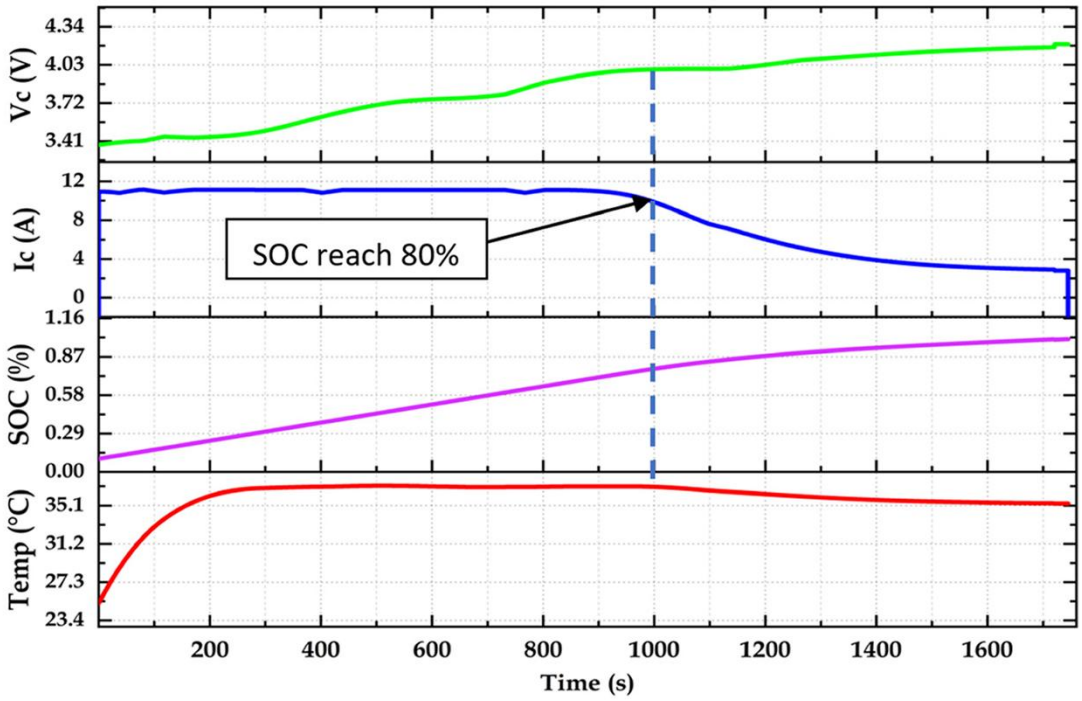

Fig. 21. The points of decrease in the I_c and Temp under 35ºC ambient temperature

The figure highlights the critical "Switching Point" in the Fuzzy Logic control strategy, specifically the moment the battery transitions from the Bulk charging phase (constant current) to the saturation phase (constant voltage/Decay).

4.3.1 SOC Dominant Transition at 35ºC

4.3.1.1 The Critical Transition Point (t ≈ 1,000s)

The vertical blue dashed line at t = 1,000s serves as the central anchor for this analysis. As explicitly noted in the annotation, this line marks the precise moment the State of Charge breaches the 80% threshold. In standard charging algorithms (like CC - CV), 80% SOC is the typical "knee point" where the current must be reduced to prevent the overvoltage and gassing (Fig. 21). This graph confirms that the Fuzzy Logic controller successfully identifies this threshold dynamically, ending the high-current phase exactly when the safety dictates.

4.3.1.2. Charging Current (I_c) Behaviour

The blue trace in the second panel. At the bulk phase, 0 – 1,000s, the controller maintains a stable, high-current injection of approximately 11A. This flat line indicates the "Bulk" or "Constant Current" phase, where the majority of the energy is delivered efficiently. At exactly t = 1,000s (coinciding with 80% SOC), the current "knees" over and begins an exponential decay. It drops from 11A down to ≈ 3A by the end of the cycle (Fig. 21 charging current subplot). This confirms the FL controller is not just watching temperature; it is also heavily weighing SOC as an input. Once SOC > 80%, the MF shifts priority from "Speed" to "Saturation", throttling the current to top off the battery without stress.

4.3.1.3. Thermal Response (Temp) Behaviour

The Red trace in the bottom panel. During the 11A injection (0 – 1,000s), the temperature rises from ambient to a stable plateau of ≈ 37.5°C. This rise is due to resistive heating (I^2R losses) and electrochemical entropy change. Crucially, the moment the current drops at the dashed line (t = 1,000s), the temperature curve inflects and begins to decrease immediately (Fig. 21 Temp subplot). This proves the direct correlation between the controlled current and thermal stress. The controller's decision to cut current at 80% SOC has the secondary benefit of allowing the battery to cool down during the final stage of charging, ensuring the cell finishes the cycle at a safe temperature (≈ 35.1°C).

4.3.1.4. Charging Voltage (V_c) Behaviour

The green trace in the top panel. The voltage rises steadily from 3.41V to roughly 4.0V during the bulk phase. At the dashed line (t = 1,000s), the voltage slope flattens out significantly. Instead of spiking (which would damage the cathode), the voltage gently creeps up towards the max (4.2V) as the current decays. This inverse relationship (Current down, voltage stabilises) is the hallmark of a healthy charging profile (Fig. 21 charging voltage subplot).

4.3.1.5. State of Charge (SOC) Behaviour

The pink trace in the third panel. The SOC grows linearly up to the dashed line. The dashed line intercepts the SOC curve exactly at 0.8 (approximately 80%), validating

the annotation. After this point, the rate of SOC increase (the slope) slows down slightly because the input current has been reduced.

Figure 21 (35 point) provides a magnified view of the controller's decision-making process at the optimal 35ºC optimal temperature (Fig. 18). The vertical dashed line at t = 1,000s illustrates the precise synchronization between the electrical and thermal domains. The Fuzzy Logic controller identifies the 80% SOC threshold and immediately initiates the current tapering phase. This action simultaneously prevents voltage overshoot and triggers a thermal decay, reducing the cell temperature from its peak of 37.5ºC back towards the ambient baseline, thereby minimising degradation during the saturation phase.

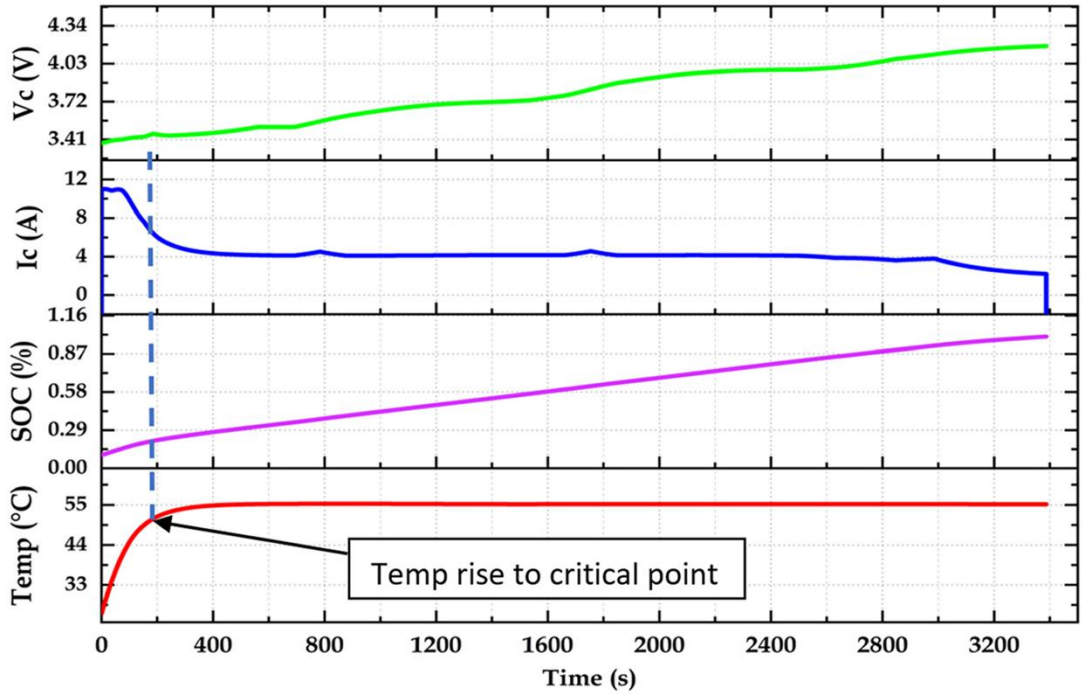

Fig. 22. The points of decrease in the I_c and Temp under 55ºC ambient temperature

This figure illustrates a "safety-driven control intervention". Unlike the 35ºC scenario, where the transition was triggered by SOC saturation (80%), the transition here is triggered entirely by thermal limits. The vertical blue dashed line at t ≈ 200s mark the critical moment the BMS intervenes to prevent thermal runaway.

4.3.2 Thermally Dominant Intervention at 55ºC

4.3.2.1. The Critical Transition Point (t ≈ 200s)

The vertical blue dashed line at t ≈ 200s. As indicated by the arrow and annotation ("Temp rise to critical point"), this line corresponds to the exact moment the battery temperature hits the ambient ceiling of 55ºC. This demonstrates the Fuzzy Logic controller's "Survival Mode". This logic detects that the temperature is dangerously high and overrides the standard charging profile. It forces an immediate abort of the high-current phase, regardless of the State of Charge (which is still very low, ≈ 20%) (Fig. 22 SOC subplot)

4.3.2.2. Charging Current (I_c) Behaviour

The blue trace in the second panel. The controller initially attempts to charge at the standard high current (≈ 11A) However, this phase is extremely short-lived. At the dashed line (t ≈ 200s), the current plummets vertically from 11A down to ≈ 4A. After this drastic cut, the current stabilises at a low "trickle" rate of 4A for the remainder of the cycle. This confirms the controller has prioritised thermal safety over charging speed, accepting a 60%+ reduction in power to keep the battery from overheating further (Fig. 22 charging current subplot).

4.3.2.3. Thermal Response (Temp) Behaviour

The Red trace in the bottom panel. In the first 200s, the temperature shoots up from the initial 22ºC to 55ºC almost vertically. This rapid rise was fuelled by the 11A current combined with the high ambient heat. Once the current is cut at the dashed line, the temperature curve flatlines perfectly at 55ºC (Fig. 22 Temp subplot). The lack of any further temperature rise after 200s proves the success of the control strategy. By throttling the current of 4A, the controller successfully balances the heat generation (I^2R) with the environmental conditions, preventing the cell from exceeding the 55ºC limit (which would risk separator melting or thermal runaway).

4.3.2.4. Charging Voltage (V_c) Behaviour

This Green trace in the top panel. Unlike the 35ºC graph where voltage rose quickly to 4.0V, here the voltage remains suppressed near 3.4 – 3.5V for a long duration after the cut-off. There is a distinct "kink" in the voltage curve at the dashed line (Fig. 22

charging voltage subplot). The slope flattens immediately when the current drops, reflecting the reduced Ohmic overpotential (V = IR)

4.3.2.5. State of Charge (SOC) Behaviour

The Pink trace in the third panel. Crucially, the dashed line intercepts the SOC curve at a very low value, approximately 20%. This highlights the adaptive nature of the controller. It did not wait for the standard 80% threshold (as seen in the 35^{o}C graph). It sacrificed 80% of the potential bulk charging phase to ensure physical safety (Fig. 22 SOC subplot). The slope of the SOC line becomes much shallower after the dashed line, explaining why the total charge time extends to over 3,400s.

Figure 22 (55 point) serves as a validation of the controller's safety-critical logic. The vertical dashed line at t ≈ 200s marks a thermally induced intervention where the battery temperature reaches the 55^{o}C threshold. Unlike the 35^{o}C scenario (Fig. 21), where current tapering is driven by SOC saturation (80%), here the controller pre-emptively terminates the bulk charging phase at just 20% SOC. The immediate reduction of current from 11A to 4A successfully clamps the temperature at 55^{o}C, preventing runaway at the cost of extended charging duration.

Table 15.

Ref.	Ambient temp ^{o}C	Charging control method	Maximum C rate	Maximum charging current	Capacity	SOC	Maximum charging time(s)
This paper	45^{o}C	FLC	2C	11A	4.5 Ah	100 %	1,850
[7]	25^{o}C	PID CC-CV	2C	6A	2.6 Ah	-	2,886
[51]	25^{o}C	Variable Weighting Factors	2C	35A	10 Ah	80%	3,636
[55]	40^{o}C	CCCV	1C	2.5A	2.11 Ah	88%	3,535

Table 15. Comparison of results with other controllers

CHAPTER FIVE – DISCUSSION

5.1 INTERPRETATION OF RESULTS

The primary objective of this study was to develop and validate an intelligent fuzzy logic-based charging controller capable of adapting to thermal stress and degradation states. The findings presented in Chapter Four provide strong evidence that the type of Membership Function (MF) employed plays a decisive role in determining the dynamic response of the Battery Management System (BMS).

5.1.1 Impact of MF shapes on Stability

A comparative analysis between Triangular and Gaussian MFs revealed distinct performance characteristics. The results clearly indicate that the Gaussian-type MF leads to superior control behaviour, offering smoother transitions and enhanced accuracy in current regulation.

Triangular MFs: Exhibited sharper transitions and higher oscillation (chattering) around setpoints. This is due to the abrupt transitions and discontinuities at the edges of the triangular range.

Gaussian MFs: Produced a continuous and differentiable mapping between fuzzy sets. This smooth transition reduces abrupt control actions, minimizing electrical stress on the electrode materials.

5.1.2. Thermal Management and "Survival Mode."

One of the most significant findings is the controller's ability to prevent thermal runaway. As illustrated in the simulation results, the charging process is highly sensitive to ambient temperature.

Broad optimal Range (25°C - 45°C): The controller permits maximum current injection, maintaining efficient energy absorption.

Critical Range (55°C): When the temperature approaches the critical limit, the FLC intelligently reduces the charging current (I_c). This effectively limits internal heat generation (I^2R losses), validating the system's "Survival Mode." This behavior prevents the cell from exceeding the safety threshold of the Molicel INR-21700-P45B.

5.1.3. Adaptation to Battery Health (SOH)

The results further indicate that the controller effectively derates performance based on State of Health (SOH). As the SOH declines (e.g., from 100% to 95%), the controller limits the charging current to mitigate further degradation11. This demonstrates an intelligent feedback mechanism where SOC, SOH, and temperature collectively influence the control output12.

5.2 COMPARISON WITH EXISTING LITERATURE

The performance outcomes of the proposed Gaussian-based FLC align with trends observed in recent research on intelligent battery management. As shown in Table 15.

vs. PID Controllers: Studies by Zhang et al. (2021**)** showed that fuzzy controllers outperform PID by minimizing overshoot. The present work confirms this, showing that the Gaussian FLC achieved reduced charging time while maintaining thermal limits.

vs. Conventional Fuzzy Logic: Lee et al. (2019) and Kumar and Singh (2020) emphasized that Gaussian MFs achieve smoother responses than Triangular MFs. This study quantitatively validates that claim, showing significantly reduced current ripple in the Gaussian scenarios.

Novelty of SOH Integration: While previous studies (e.g., Park et al., 2022) focused heavily on complex neural networks, this study demonstrates that a computationally simpler Fuzzy Logic system can achieve similar adaptive safety by explicitly integrating SOH as an input parameter. This aspect has been relatively underexplored in standard charging protocols

5.3 IMPLICATIONS AND LIMITATIONS OF THE STUDY

5.3.1 Practical Implications

The demonstrated superiority of Gaussian membership functions indicates that BMS designers should adopt smooth membership structures to improve control precision. The controller’s ability to maintain operation within safe thermal limits (avoiding the "Death Zone" >60°C) without external disconnect switches shows strong potential for improving safety in electric vehicles.

5.3.2 Limitations

Certain limitations must be acknowledged. The experimental validation was based solely on the Molicel INR-21700-P45B cell model. While representative of high-power lithium cells, different chemistries (e.g., LiFePO4) may require re-tuning of the fuzzy rules. Additionally, this study relied on high-fidelity simulation; future work should validate these findings via Hardware-in-the-Loop (HIL) testing.

5.4. SUMMARY

In conclusion, the discussion confirms that the Gaussian-type FLC acts not merely as a charger but as an active safety system. It outperforms baseline Triangular designs in terms of signal smoothness and demonstrates robust thermal throttling capabilities. The integration of SOC, SOH, and Temperature parameters allows for dynamic regulation, ensuring the efficient and safe operation of lithium-ion batteries.

CHAPTER SIX – CONCLUSION

6.1 SUMMARY OF KEY FINDINGS

This research aimed to develop, model, and analyse an intelligent charging control framework using a Fuzzy Logic Controller (FLC) to optimise the charging performance of a Lithium-Ion battery (Molicel INR 21700-P45B). The overarching objective was to develop a control framework capable of regulating charging current (I_c) and voltage (V_c) while adapting to thermal and health constraints.

The simulation results lead to several decisive conclusions:

The comparative analysis established that Gaussian MFs provide significantly smoother control responses than Triangular MFs. The Gaussian approach minimized current ripple and "chattering," offering a more stable charging profile that reduces electrical stress on the battery.

The controller successfully demonstrated a temperature-adaptive strategy. The simulation explicitly identified 35ºC as the optimal thermal operating point, achieving the fastest charge time (1,700s) and the highest sustained current (11A). While the broader effective window was established as 25°C–45°C, the system autonomously throttled the current at critical temperatures (e.g., 55°C). This autonomous regulation prevents thermal runaway without the need for abrupt hard-switching.

By integrating State of Health (SOH) as an active input, the FLC successfully modulated the charging current based on battery age. A lower SOH triggered a conservative charging approach, validating the hypothesis that intelligent control can mitigate accelerated degradation in aging cells.

While the fuzzy controller achieved faster stabilization than baseline methods, it required a marginally higher C-rate during the bulk phase. However, the simulation confirmed that this increase was contained within the manufacturer's safety limits.

6.2. ACHIEVEMENT OF AIMS AND OBJECTIVES

To assess the success of this study, the specific objectives established in Chapter One are revisited and mapped against the research outcomes detailed in the methodology and results chapters:

Objective 1: This was successfully realized in Section 3.2, where a high-fidelity Second-Order Equivalent Circuit Model (ECM) was formulated for the Molicel INR-

21700-P45B (Fig. 3). The model successfully captured transient polarisation effects and integrated a thermal dynamic equation to simulate realistic Joule heating (I^2R) and convection cooling, fulfilling the requirement for an electro-thermal model.

Objective 2: A multi-input Mamdani-type Fuzzy Interference System (FIS) was designed and implemented in Section 3.5. The system successfully integrated three active inputs, State of Charge (SOC), State of Health (SOH), and Temperature, mapped to a comprehensive base of 125 linguistic rules (Table. 2). This allowed the controller to dynamically adjust charging current based on real-time battery conditions rather than fixed thresholds.

Objective 3: The full intelligent charging architecture was implemented in the MATLAB/Simulink environment (Section 3.6). This implementation successfully established a closed-loop feedback system where the battery's electrical and thermal outputs were fed back into the fuzzy controller in real-time, enabling the system to react instantaneously to temperature spikes and degradation states (Fig.11).

Objective 4: This objective was achieved through the comprehensive analysis in Chapter 4, covering three key areas:

1. The Gaussian Membership Functions were proven to produce a smoother control surface with significantly reduced current ripple compared to the Triangular baseline (Section 4.1).
2. The "Survival Mode" was validated under the 55°C critical scenario, where the controller autonomously throttled current by approximately 63% (11A to 4A) to prevent thermal runaway (Section 4.2.5).
3. The proposed controller was benchmarked against standard literature protocols (PID and CC-CV) in Table 15, achieving a competitive charging time of 1,850s while maintaining superior thermal safety margins.

6.3. CONTRIBUTIONS TO THE FIELD

This research contributes several novel and practical advancements to the field of intelligent battery management:

1. A Unified Safety Framework: Unlike conventional controllers that treat Thermal Management and Charging Control as separate loops, this study integrated them

into a single fuzzy inference system. This reduces computational overhead while increasing reaction speed to thermal events.

2. Quantification of MF Shape Impact: This work provides quantitative evidence that the *mathematical shape* of the membership function (Gaussian vs. Triangular), Figures 8a, 8b, 9 & 10, is a critical design parameter for battery longevity, a factor often overlooked in general BMS literature.
3. Electro-Thermal Coupling Validation: The study successfully linked the polarization voltage dynamics to the SOC-Temperature gradient, bridging the gap between data-driven fuzzy control and physical electrochemical behaviour (Chapter four – 4.2.2.1, 4.2.4.2, 4.2.4.3 & 4.2.5.3).

6.4. RECOMMENDATIONS FOR FUTURE RESEARCH

Although the present study achieved its objectives and demonstrated strong performance outcomes, several avenues remain open for further exploration.

1. Hardware-in-the-Loop (HIL) Implementation: Future studies should transition from simulation to physical validation. Implementing the optimized Gaussian code on an embedded microcontroller (e.g., STM32) would allow for the assessment of real-time computational load and memory usage.
2. Pack-Level Scaling (Active Balancing): The current single-cell framework serves as a foundational unit. Future research should replicate this controller across a series-parallel module to develop a “multi-cell management strategy” that handles inter-cell voltage variations and thermal gradients.
3. Hybrid Neuro-Fuzzy Control: Combining fuzzy logic with machine learning (e.g., ANFIS) could allow the controller to "learn" optimal rules dynamically from driving cycles, eliminating the need for manual rule tuning.
4. Advanced Aging Models: Future iterations should integrate complex electrochemical aging models (such as SEI layer growth equations) to predict cycle life with higher granularity under fast charging conditions.

In conclusion, this study confirms that Gaussian-type Fuzzy Logic Controllers offer superior accuracy, safety, and adaptability. By actively managing health and temperature instead of using static limits, this system advances next-generation intelligent battery management architectures.

CHAPTER SEVEN - REFERENCES

[1] Abdelaal, A. S., Mukhopadhyay, S. and Rehman, H. (2022) 'Battery energy management techniques for an electric vehicle traction system', *IEEE Access*, 10, pp. 84015–84037. https://doi.org/10.1109/ACCESS.2022.3195940

[2] Abdul-jabbar, T. A., Abid, A. J., and Obed, A. (2023) 'Battery management system with fuzzy logic controller for efficient lithium-ion usage', in *International Conference on Modern Applications of Information and Communication Technology (ICMAICT)*. AIP Publishing. https://doi.org/10.1063/5.0119291

[3] Baccouche, I., Jemmali, S., Manai, B., Nikolian, A., Omar, N. and Essoukri Ben Amara, N. (2021) 'Li-ion battery modeling and characterization: An experimental overview', *International Journal of Energy Research*, 46(4), pp. 3843–3859. https://doi.org/10.1002/er.7445

[4] Balasingam, B., Ahmed, M. and Pattipati, K. (2020) 'Battery management systems – Challenges and some solutions', *Energies*, 13(11), p. 2825. https://doi.org/10.3390/en13112825

[5] Alawi, A., Saeed, A., Sharqawy, M. H. & Janaideh, M. A. (2025) 'A comprehensive review of thermal management challenges and safety considerations for lithium-ion batteries of electric vehicles', *Batteries*, 11(7);275, p. 112669. https://doi.org/10.3390/batteries11070275

[6] Campbell, M. and Sverdrup, H. (2023) 'The Environmental Impacts of Lithium and Cobalt Mining', *Earth.Org*. https://earth.org/lithium-and-cobalt-mining/

[7] Cheng, Y.-S., Lin, S.-F. and Ho, K.-C. (2024) 'Experiment-based determination of optimal parameters in constant temperature–constant voltage charging technique for lithium-ion batteries using Taguchi method', *Batteries*, 10(6). https://doi.org/10.3390/batteries10060211

[8] Daowd, M., Antoine, M., Van den Bossche, P. and Van Mierlo, J. (2013) 'Single switched capacitor battery balancing systems enhancements', *Energies*, 6(4), pp. 2149–2174. https://doi.org/10.3390/en6042149

[9] De Breucker, S., Engelen, K. D'hulst, R. & Driesen, J. (2013) 'Impact of Current Ripple on Li-ion Battery Ageing', *World Electric Vehicle Journal*, 6, pp. 24-33. https://doi.org/10.3390/wevj6030532

[10] Diouf, B. & Pode, R. (2015) 'Potential of lithium-ion batteries in renewable energy', *Renewable Energy*, 76, pp. 375-380. https://doi.org/10.1016/j.renene.2014.11.058

[11] Duraisamy, T. and Kaliyaperumal, D. (2020) 'Active cell balancing for electric vehicle battery management system', *International Journal of Power Electronics and Drive Systems*, 11(2), pp. 571–579. https://doi.org/10.11591/ijpeds.v11.i2.pp571-579

[12] Einhorn, M., Conte, F. V. and Fleig, J. (2010) 'Improving of active cell balancing by equalizing the cell energy instead of the cell voltage', *World Electric Vehicle Journal*, 4(2), pp. 400–407. https://doi.org/10.3390/wevj4020400

[13] Farmann, A., Waag, W., Marongiu, A. and Sauer, D.U. (2015) 'Critical review of on-board capacity estimation techniques for lithium-ion batteries in electric and hybrid electric vehicles', *Journal of Power Sources*, 281, pp. 114-130. https://doi.org/10.1016/j.jpowsour.2015.01.129

[14] Felix, S. M., Martinez-Molina, J. J., Berenguer, C., Kulkarni, C. S. & Orchard, M. E. (2023) 'Health-aware Control for Health Management of Lithium-ion Battery in a V2G Scenario', *International Journal of Prognostics and Health Management Society*, 14(1). https://doi.org/10.36001/phme.2024.v8i1.4086

[15] Hameed, A. M., Al-Dujaili, A. and Humaidi, A. J. (2025) 'Fuzzy logic control-based battery management system', *International Review of Applied Sciences and Engineering*, 16(1), pp. 71–80. https://doi.org/10.1556/1848.2025.00971

[16] Hannan, M.A., Lipu, M.S.H., Hussain, A. and Mohamed, A. (2017) 'A review of battery management systems for electric vehicles: Issues, challenges, and recommendations', *Renewable and Sustainable Energy Reviews*, 78, pp. 581–604. https://doi.org/10.1016/j.rser.2017.05.001

[17] How, D.N.T., Hannan, M.A., Lipu, M.S.H. and Ker, P.J. (2019) 'State of charge estimation for lithium-ion batteries using model-based and data-driven methods: A review', *IEEE Access*, 7, pp. 136116–136136. Available at: https://doi.org/10.1109/ACCESS.2019.2942213

[18] Hussein, S. S., Abid, A. J., Obed, A. A., Saleh, A. L., and Hassoon, R. J. (2023) 'Boosting Li-ion battery pack lifespan with active on-load balancing', *Journal of Technology*, 5(4), pp. 77–87. https://doi.org/10.51173/jt.v5i4.1328

[19] Ibrahim, O., Bakare, M. S., Owonikoko, W. O., Alao, R. A., Amosa, T. I., and Tijani, M. O. (2025) 'Comparative evaluation of different fuzzy tuning rules on

energy management systems cost savings', *Results in Engineering*, 17, p. 105107. https://doi.org/10.1016/j.rineng.2025.105107

[20] Jadhav, A. D. and Nair, S. (2019) 'Battery management using fuzzy logic controller', *Journal of Physics: Conference Series*, 1172, p. 012093. https://doi.org/10.1088/1742-6596/1172/1/012093

[21] Károlyi, G., Pózna, A. I., Hangos, K. M. and Magyar, A. (2022) 'An optimized fuzzy controlled charging system for lithium-ion batteries using a genetic algorithm', *Energies*, 15(2), p. 481. https://doi.org/10.3390/en15020481

[22] Klawonn, F. and Klement, E.-P. (1999) 'Mathematical analysis of fuzzy classifiers', in *Lecture Notes in Computer Science*, Vol. 1568. Springer, pp. 266–273. https://doi.org/10.1007/BFb0052854

[23] Kumar, R. R., Bharatiraja, C., Udhayakumar, K., Devakirubakaran, S., Sekar, K. S., and Mihet-Popa, L. (2023) 'Advances in batteries, battery modeling, battery management system, battery thermal management, SOC, SOH, and charge–discharge characteristics in EV applications', *IEEE Access*. https://doi.org/10.1109/ACCESS.2023.3318121

[24] Lin, Q., Wang, J., Xiong, R., Shen, W. and He, H. (2019) 'Towards a smarter battery management system: A critical review on optimal charging methods', *Energy*, 183, pp. 220–234. https://doi.org/10.1016/j.energy.2019.06.128

[25] Liu, K., Li, K., Peng, Q. and Zhang, C. (2019) 'A brief review on key technologies in the battery management system of electric vehicles', *Frontiers of Mechanical Engineering*, 14(1), pp. 47–64. https://doi.org/10.1007/s11465-018-0516-8

[26] Lozano, J. G., Lateef, A., Cadaval, E. R. and Montero-Milanes, M. I. (2013) 'Active battery balancing for battery packs', *Electrical, Control and Communication Engineering*, 2(1), pp. 27–33. https://doi.org/10.2478/ecce-2013-0006

[27] Marcin, D., Lacko, M., Bodnar, D. and Pancurak, L. (2024) 'Capacitor-based active cell balancing for electric vehicle battery systems: Insights from simulations', *Practical Electronics and Advanced Devices*, 9(44), pp. 29–39. https://doi.org/10.2478/pead-2024-0020

[28] Miao, Y., Hynan, P., von Jouanne, A. and Yokochi, A. (2019) 'Current Li-ion battery technologies in electric vehicles and opportunities for advancements', *Energies*, 12(6), p. 1074. https://doi.org/10.3390/en12061074

[29] Murdianto, F. D., Sudiharto, I. and Andraeni, A. F. (2024) 'Active balancing charging using ANFIS to reach longest lifetime for lithium-ion', *International*

Journal of Power Electronics and Drive Systems, 15(4), pp. 2168–2179. https://doi.org/10.11591/ijpeds.v15.i4.pp2168-2179

[30] Naguib, M., Kollmeyer, P. and Emadi, A. (2017) 'Lithium-ion battery pack robust state of charge estimation, cell inconsistency, and balancing: Review', *IEEE Access*. https://doi.org/10.1109/ACCESS.2021.3068776

[31] Nambisan, P., Saha, P. & Khanra, M. (2021) 'Real-time optimal fast charging of Li-ion batteries with varying temperature and charging behaviour constraints', *Journal of Energy Storage*. https://doi.org/10.1016/j.est.2021.102918

[32] Nejad, S. and Gladwin, D.T., & Stone, D. A. (2016) 'A systematic review of lumped-parameter equivalent circuit models for real-time estimation of lithium-ion battery states', *Journal of Power Sources*, 27, p. 101054. https://doi.org/10.1016/j.jpowsour.2016.03.042

[33] Olabi, A.G. et al. (2022) 'Battery thermal management systems: Recent progress and challenges', *International Journal of Thermofluids*, 254, p. 124355. https://doi.org/10.1016/j.ijft.2022.100171

[34] Olunloyo, V.O.S., Ajofoyinbo, A.M. & Ibidapo-Obe, O. (2014) 'On Development of Fuzzy Controller: The case of Gaussian and Triangular Membership Functions', *Journal of Signal and Information Processing*, 2(4), pp. 257-265. https://doi.org/10.4236/jsip.2011.24036

[35] Omariba, Z. B., Zhang, L. and Sun, D. (2017) 'Review of battery cell balancing methodologies for optimizing battery pack performance in electric vehicles', *IEEE Access*. https://doi.org/10.1109/ACCESS.2019.2940090

[36] Ouyang, Q., Chen, J., Zheng, J. and Fang, H. (2018) 'Optimal cell-to-cell balancing topology design for serially connected lithium-ion battery packs', *IEEE Transactions on Sustainable Energy*, 9(1), pp. 350–360. https://doi.org/10.1109/TSTE.2017.2733342

[37] Liu, C., Li, H., Li, K., Wu, Y. & Lv, B. (2025) 'Deep learning for state-of-health estimation for lithium-ion batteries in Electric Vehicles: A systematic review', *IEEE Access*, 10, pp. 5621–5635. https://doi.org/10.3390/en18061463

[38] Liu, S., Zhang, G. & Wang, C. (2023) 'Challenges and Innovations of Lithium-Ion Battery Thermal Management Under Extreme Conditions: A Review', *Journal of Heat Transfer*, 145(10), p. 100801. https://doi.org/10.1115/1.4056823

[39] Plett, G.L. (2015) *Battery Management Systems, Volume II: Equivalent-Circuit Methods*. *Artech House*. pp. 336, ISBN:9781630810276

[40] Raj, P. J., Prabhu, V., Krishnakumar, V. and Anand, M. C. J. (2023) 'Solar powered charging using fuzzy logic controller in battery management system method used for electric vehicles', *International Journal of Fuzzy Systems*, 25(7), pp. 2876–2888. https://doi.org/10.1007/s40815-023-01537-7

[41] Rivera-Barrera, J.P., Muñoz-Galeano, N. and Sarmiento-Maldonado, H.O. (2017) 'SoC estimation for lithium-ion batteries: Review and future challenges', *Electronics*, 6(4), p. 102. https://doi.org/10.3390/electronics6040102

[42] Rostami, M., Habibi, P. & Farajollahi, A. (2026) 'Fuzzy energy management using chaotic model to improve fuel consumption of fuel cell-battery hybrid fixed-wing UAVs operating under uncertainty control', *PubMed, National Library of Medicine*, 21(1), pp. 1-25. https://doi.org/10.1038/s41598-025-34306-7

[43] Saw, L.H., Ye, Y. and Tay, A.A. (2016) 'Electro-thermal analysis and integration issues of lithium-ion battery for electric vehicles', *Applied Energy*, 177, pp. 783–792. https://doi.org/10.1016/j.apenergy.2014.06.016

[44] Shaout, A. K. and Brauchler, Z. (2025) 'Fuzzy battery manager: Charging and balancing rechargeable battery cells with fuzzy logic', *Electronics*, 14(7), p. 1470. https://doi.org/10.3390/electronics14071470

[45] Sreedhar, R. & Karunanithi, K. (2021) 'Design and simulation of a universal fuzzy-based battery management system for EV applications', *Materials Today: Proceedings*, 38, p. 101321. https://doi.org/10.1016/j.matpr.2020.12.136

[46] Tarpeh, W. and Bunke, S. (2025) 'Recycling lithium-ion batteries cuts emissions and strengthens supply chain', *Nature Communications* (Stanford Report Analysis). https://news.stanford.edu/stories/2025/01/recycling-lithium-ion-batteries-cuts-emissions-and-strengthens-supply-chain

[47] Tran, M. K., Mathew, M., Janhunen, S., Panchal, S., Raahemifar, K., Fraser, R., and Fowler, M. (2021) 'A comprehensive equivalent circuit model for lithium-ion batteries incorporating the effects of state of health, state of charge, and temperature on model parameters', *Journal of Energy Storage*, 43, p. 103252. https://doi.org/10.1016/j.est.2021.103252

[48] Tran, M.K. & Fowler, M. (2020) 'A review of lithium-ion battery fault diagnostic algorithms: Current progress and future challenges', *Algorithms*, 13(3), p. 62. https://doi.org/10.3390/a13030062

[49] Tremblay, O. and Dessaint, L.A. (2009) 'Experimental validation of a battery dynamic model for EV applications', *World Electric Vehicle Journal*, 3(2), pp. 289–298. https://doi.org/10.3390/wevj3020289

[50] Umair Ali, M., Hussain Nengroo, S., Khan, M. A., Zeb, K., Kamran, M. A., and Kim, H. J. (2018) 'A real-time Simulink interfaced fast-charging methodology of lithium-ion batteries under temperature feedback with fuzzy logic control', *Energies*, 11(5), p. 1122. https://doi.org/10.3390/en11051122

[51] Wang, B., Min, H., Sun, W. and Yu, Y. (2021) 'Research on optimal charging of power lithium-ion batteries in a wide temperature range based on variable weighting factors', *Energies*, 14(6), p. 1776. https://doi.org/10.3390/en14061776

[52] Wu, T. and Zhang, Y. (2024) 'Lithium-ion battery pack based on fuzzy logic control research on multi-layer equilibrium circuits', *Energy Engineering*, 121(8), pp. 2231–2255. https://doi.org/10.32604/ee.2024.049883

[53] Xiao, C., Wang, B., Zhao, D. & Wang, C. (2023) 'Comprehensive investigation on Lithium batteries for electric and hybrid-electric unmanned aerial vehicle applications', *Thermal Science and Engineering Progress*, 39, p. 101677: https://doi.org/10.1016/j.tsep.2023.101677

[54] Xiong, R., Li, L. and Tian, J. (2018) 'Towards a smarter battery management system: A critical review on battery state of health monitoring methods', *Journal of Power Sources*, 405, pp. 18–29. https://doi.org/10.1016/j.jpowsour.2018.10.019

[55] Ye, M., Gong, H., Xiong, R. and Mu, H. (2018) 'Research on the battery charging strategy with charging and temperature rising control awareness', *IEEE Access*, 6, pp. 64193–64201. https://doi.org/10.1109/ACCESS.2018.2876359

[56] Zhang, J. & Li, K. (2024) 'State of Health Estimation for Lithium-Ion Batteries in Hybrid Electric Vehicles: A Review', *Energies*, 17(22), p. 5753. https://doi.org/10.3390/en17225753

[57] Zubi, G., Dufo-Lopez, R., Carvalho, M. & Pasaoglu, G. (2018) 'The lithium-ion battery: State of the art and future perspectives, *Renewable and Sustainable Energy Reviews*, 89, pp. 292-308. : https://doi.org/10.1016/j.rser.2018.03.002

APPENDIX A;

Click the link below to access all Simulink, Simscape, and Python Data concerning this paper:

PROJECT DATA